The role of standardisation in deformation imaging and early detection of cardiotoxicity in patients undergoing chemotherapy using speckle tracking

Ph.D. Thesis

by

Adrienn Tünnemann-Tarr, M.D.

Szeged, Hungary

2021

The role of standardisation in deformation imaging and early detection of cardiotoxicity in patients undergoing chemotherapy using speckle tracking

Ph.D. Thesis

by

Adrienn Tünnemann-Tarr, M.D.

Supervisor:

Prof. Albert Varga M.D. Ph.D.

The experimental and clinical investigation of heart diseases

Second Department of Medicine and Cardiology Centre

University of Szeged

Szeged, Hungary

2021

Table of contents

Publications related to the thesis:

I. **Tarr A**, Stöbe S, Trache T, Kluge J-G, Varga A, Pfeiffer D, Hagendorff A. The impact of foreshortening on regional strain - a comparison of regional strain evaluation between speckle tracking and tissue velocity imaging. Ultraschall Med. 2013;34:446–53. Impact factor:4,645

II. **Tarr A,** Stoebe S, Tuennemann J, Baka Z, Pfeiffer D, Varga A, Hagendorff A. Early detection of cardiotoxicity by 2D and 3D deformation imaging in patients receiving chemotherapy. Echo Res Pract. 2015;2:81–8.

Other publications not directly related to the thesis:

Tarr A, Csanády M, Hőgye M, Sári G, Sepp R, Forster T. Korszerű kezeléssel elért eredményeink összehasonlítása a familiáris dilatatív és sporadikus dilatatív cardiomyopathiás betegeinkben. Bulletin of medical sciences/Orvostudományi értesítő. 2009;82:95-98.

Kluge J-G, Hagendorff A, Pfeiffer D, Jurisch D, **Tarr A**. Active infective prosthetic endocarditis after percutaneous edge-to-edge mitral valve repair. Eur J Echocardiogr. 2011;12:710. Impact factor:2.317

Kluge J-G, Jurisch D, **Tarr A**, Hagendorff A, Pfeiffer D. Right atrial free-floating thrombus in dilated cardiomyopathy. Eur J Echocardiogr. 2011;12:798. Impact factor: 2.317

Hagendorff A, Stoebe S, **Tarr A**, Pfeiffer D. Die konventionelle Standarduntersuchung in der transthorakalen Echokardiografie bei Patienten mit degenerativer Aortenklappenstenose. [Standard transthoracic echocardiography examination in patients with degenerative stenosis of the aortic valve]. Ultraschall Med. 2012;33:520-38. Impact factor: 4.116

Hagendorff A, Stöbe S, **Tarr A**, Pfeiffer D. Spezielle echokardiografische Diagnostik und besondere Problemkonstellationen bei Patienten mit degenerativer Aortenklappenstenose. [Special echocardiographic diagnosis and specific problem constellations in patients with degenerative stenosis of the aortic valve]. Ultraschall Med. 2013;34:214-32. Impact factor: 4.645

Trache T, Stöbe S, **Tarr A**, Pfeiffer D, Hagendorff A. The agreement between 3D, standard 2D and triplane 2D speckle tracking: effects of image quality and 3D volume rate. Echo Res Pract. 2014;1:71–83.

Stoebe S, **Tarr A**, Pfeiffer D, Hagendorff A. The impact of the width of the tracking area on speckle tracking parameters-methodological aspects of deformation imaging. Echocardiography. 2014;31:586–96. Impact factor: 1.254

Hagendorff A, Stoebe S, **Tarr A**, Pfeiffer D. Standardized transthoracic echocardiography in patients with primary and secondary mitral valve regurgitation. Ultraschall Med. 2015;36:10–34. Impact factor: 4.434

Katzmann JL, **Tünnemann-Tarr A**, Laufs U. Europäische Leitlinien zu Lipiden 2019 : Was ist neu? [European dyslipidemia guidelines 2019 : What is new?]. Herz. 2019;44:688–95. Impact factor: 1.033

Tünnemann-Tarr A, Stöbe S, Laufs U, Hagendorff A, Tayal B. Speckle tracking echocardiography in a patient with viral myocarditis and acute myocardial infarction. J Cardiol Cases. 2020;22:184–91.

Stöbe S, Tayal B, **Tünnemann-Tarr A**, Hagendorff A. Dynamics in myocardial deformation as an indirect marker of myocardial involvement in acute myocarditis due to HIV infection: a case report. Eur Heart J Case Rep. 2021;5:ytaa511.

Katzmann JL, Lehmann M, **Tünnemann-Tarr A**, Haack I an, Dressel A, März W, Laufs U. Cutaneous manifestations in familial hypercholesterolaemia. Atherosclerosis. 2021;333:116–23. Impact factor:5.162

Tünnemann-Tarr A, Scharnagl H, Katzmann JL, Stürzebecher P, Laufs U. Familial chylomicronemia syndrome due to a heterozygous deletion of the chromosome 8 treated with the apoCIII inhibitor volanesorsen: A case report. Medicine (Baltimore). 2021;100:e27573. Impact factor: 1.889.

Total Impact factor: 27.167

Abbreviations

ASE	American Society of Echocardiography
BNP	brain Natriuretic Peptide
5ChV	five chamber view
4ChV	four chamber view
CMR	cardiac magnetic resonance
CTLA-4	cytotoxic T lymphocyte-associated antigen 4
2D	2-dimensional
3D	3-dimensional
4D	4-dimensional
DNA	deoxyribonucleic acid
EACVI	European Association of Cardiovascular Imaging
ECG	electrocardiography
echo	echocardiography
fps	frames per second
5-FU	5-fluorouracil
GCS	global circumferential strain
GLS	global longitudinal strain
GRS	global radial strain
HER2	human epidermic growth factor receptor-2
HF	heart failure
hs-cTn	high-sensitivity cardiac troponin
IL-6	interleukin-6
LGE	late gadolinium enhancement
LV	left ventricular
LVEDV	left ventricular end-diastolic volume
LVESV	left ventricular end-systolic volume
LVEF	left ventricular ejection fraction
MAB	monoclonal antibody
MAP-kinase	mitogen-activated protein kinase
MPO	myeloperoxidase
MuRF1	muscle RING-finger protein-1
MyHCα	myosin heavy chain-α
MyHCβ	myosin heavy chain-β
NADPH	nicotinamide adenine dinucleotide phosphate
NOS	nitrit oxide synthase
NCS-1	neuronal calcium sensor 1
NT-Pro BNP	N-terminal pro-B-type natriuretic peptide

MI	myocardial infarction
PD-1	programmed cell death 1
PD-L1	programmed cell death ligand 1
PSS	peak systolic strain
RNA	ribonucleic acid
ROI	region of interest
ROS	reactive oxygen species
RNS	reactive nitrogen species
RT	radiotherapy
SAD	sum of absolute differences
SR	strain rate
ST	speckle tracking
STE	speckle tracking echocardiography
TDI	tissue Doppler imaging
TNF-alpha	tumour necrosis factor alpha
TVI	tissue velocity imaging
VEGF	vascular endothelial growth factor

1 Introduction

Echocardiography is a non-invasive method to study the morphology and function of the heart and its structures, which has been developing since 1953. From M-mode imaging through B-mode, Doppler, and colour echocardiography to deformation imaging and 3D/4D echocardiography, all these modalities are now included in the routine imaging of the heart.

The advantages of these methods are non-invasiveness, being radiation-free and favourable cost-effectiveness. Echocardiography is therefore a technique that can enable diagnosis in experienced hands or supplement other non-invasive and invasive procedures. It can perfectly be integrated into the diagnostic chain, can assist therapeutic decision making and it may even abrogate the necessity of further operations.

The main cornerstone of this technique is image quality, influenced by the echocardiographic equipment, the patient's body structure and the systematic approach of the examiner (structured flow of examination). Therefore, there is a need for standardisation, which will definitely improve the diagnostic process and the detection of pathological conditions even in case of poor image quality.

1.1 Standardisation of echocardiography

The standardisation of the examination results in reproducibility, low intra-observer and inter-observer variability. Due to reproducibility, relevant information and correctly measured values can be collected that enables a proper diagnosis. In addition, appropriate standardisation indicates the competence of the investigator [1]. For this reason, international cardiology committees regularly make recommendations to promote technical progress [2, 3]. Recent studies have also attempted to standardise the values of echocardiographic measurements [4].

The lack of standardisation has made the development of appropriate echocardiographic software challenging. Thus, it is important to reduce inter-observer variability evoked by the use of specific postprocessing software enabling objective and reproducible image analysis. In particular, deformation imaging requires interpretation of software-independent values in 2-dimensional (2D) echocardiography and 3-dimensional (3D) echocardiography echocardiography. Current studies have demonstrated that the strain measurements of deformation imaging have improved significantly after standardisation [5].

1.2 Myocardial mechanics: fibre network of the left ventricle

The anatomical complexity of the myocardial fibre network enables the highly complicated movements of the heart. The muscles of the ventricles are divided into three layers: the outer oblique layer, the central circular layer and the inner longitudinal layer [5, 6]. In the left ventricle the fibres of the subepicardium run from the annulus fibrosus in a left-handed direction, in the mid layer they are oriented in a circumferential pattern, while in the subendocardium they run in a right-handed direction [7]. The myocardial fibres are connected to each other. Due to their cyclic shortening and lengthening, specific patterns of deformation can be observed throughout the cardiac cycle. The contraction of these three layers causes longitudinal, radial, and circumferential movements of the heart, moreover, a contortion of the myocardium is also evoked by torsion, twist and untwist during systole and diastole.

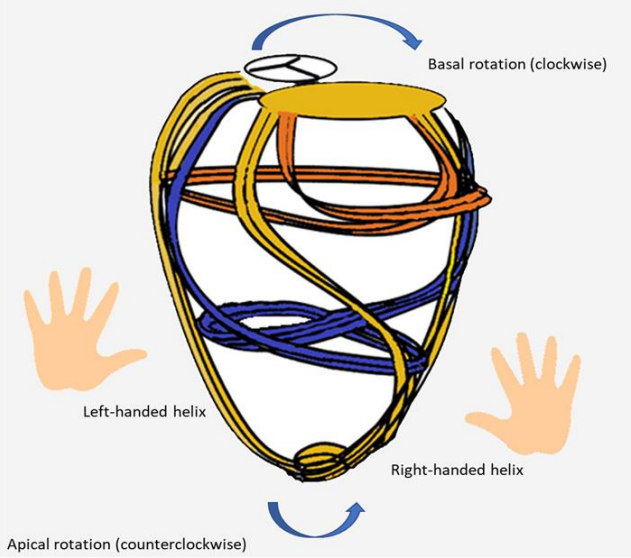

Figure 1. ***Myocardial fibre orientation and direction of rotation*** The myocardial fibres of the subepicardium mostly run helically in a left-handed direction, the fibres of the mid layer run circumferentially in a missing net rotation, while the fibres of the subendocardium mostly run helically in a right-handed direction.

1.3 Deformation imaging: strain

Deformation or strain imaging is an echocardiographic method to describe and analyse myocardial motion. Strain is a dimensionless physical term, which expresses by what

percentage a basic value of an object related to its original shape has changed. It is used in cardiac visualisation for the measurement of the morphological alteration of the heart muscle. For a one-dimensional object, the only possible deformation is lengthening or shortening (Figure 2). The numerical description of strain includes the Lagrangian and Eulerian (natural) method. They are defined by the following mathematical formulas, respectively: $\varepsilon=(L1-L0)/L0=\Delta L/L0$ and $\acute{\varepsilon}= \ln(L1/L0)$ where symbol ε is used for the description of Lagrangian strain and L0, L1, ΔL mean the original length, final length, and the change in length, respectively. Symbol $\acute{\varepsilon}$ describes natural strain. In clinical practice natural strain is more commonly used.

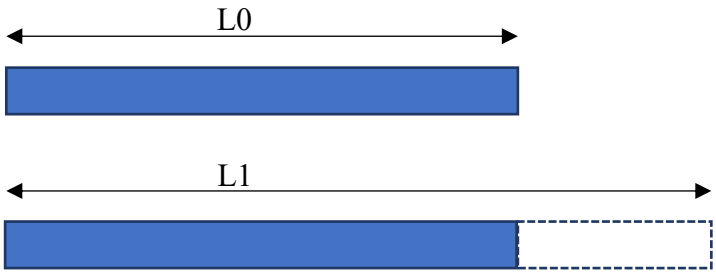

Figure 2. ***Deformation of an object*** L0: original length, L1: final length

The values of strain can be positive, negative or zero corresponding to lengthening, shortening or no change in length, respectively. The extent of natural strain is smaller for positive values and larger for negative values, compared to the Lagrangian strain [8]. The strain rate (SR) is the change in strain over time (i.e., the rate of deformation) calculated as change in strain ($d\varepsilon$) per change in time (dt), and expressed in units s^{-1}.

In 2D echocardiography, there might be shear strains in addition to normal strain in the imaging plane. Shear strains are measured as a consequence of changes in the angle.

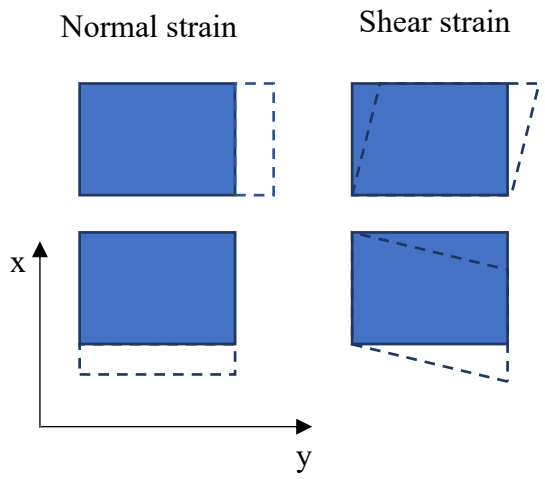

Figure 3. ***Normal strain and shear strain*** By normal strain the change occurs along the x and y axis, while by shear strain there is a parallelogram shaped displacement of the opposite borders.

Three types of strain values can be measured during the 3D movement of the heart. Longitudinal strain is the deformation of the left ventricle from the annular ring to the apex. As physiologically the length of the left ventricle (L) is shorter than its original length (L0) during systole, the normal values are negative.

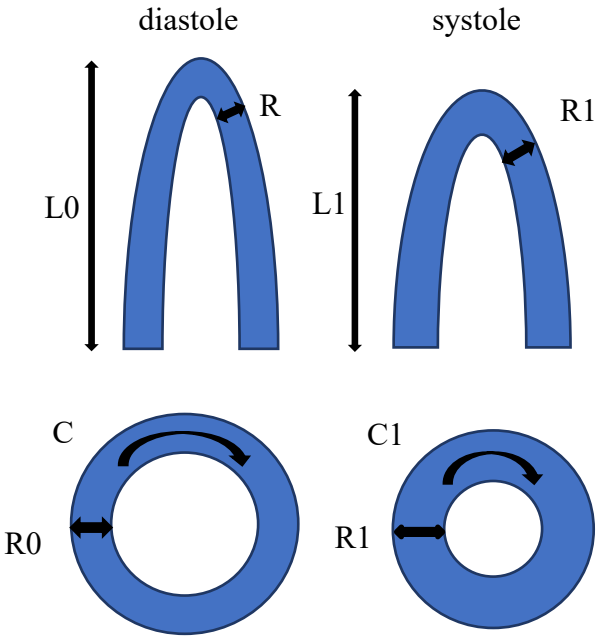

Figure 4. ***The deformation of the left ventricle during the cardiac cycle*** Longitudinal shortening: L0-L1, radial thickening: R0-R1 and circumferential shortening: C0-C1.

Radial strain is the expression of the radial contraction or thickening of the left ventricular wall. It is positive in healthy individuals because the left ventricular wall thickness increases during systolic contraction. Circumferential strain represents the myocardial contraction along the circular contour and the short axis. It is negative in healthy individuals since the circumference of the left ventricle decreases during systole (Figure 4, 5 and 6).

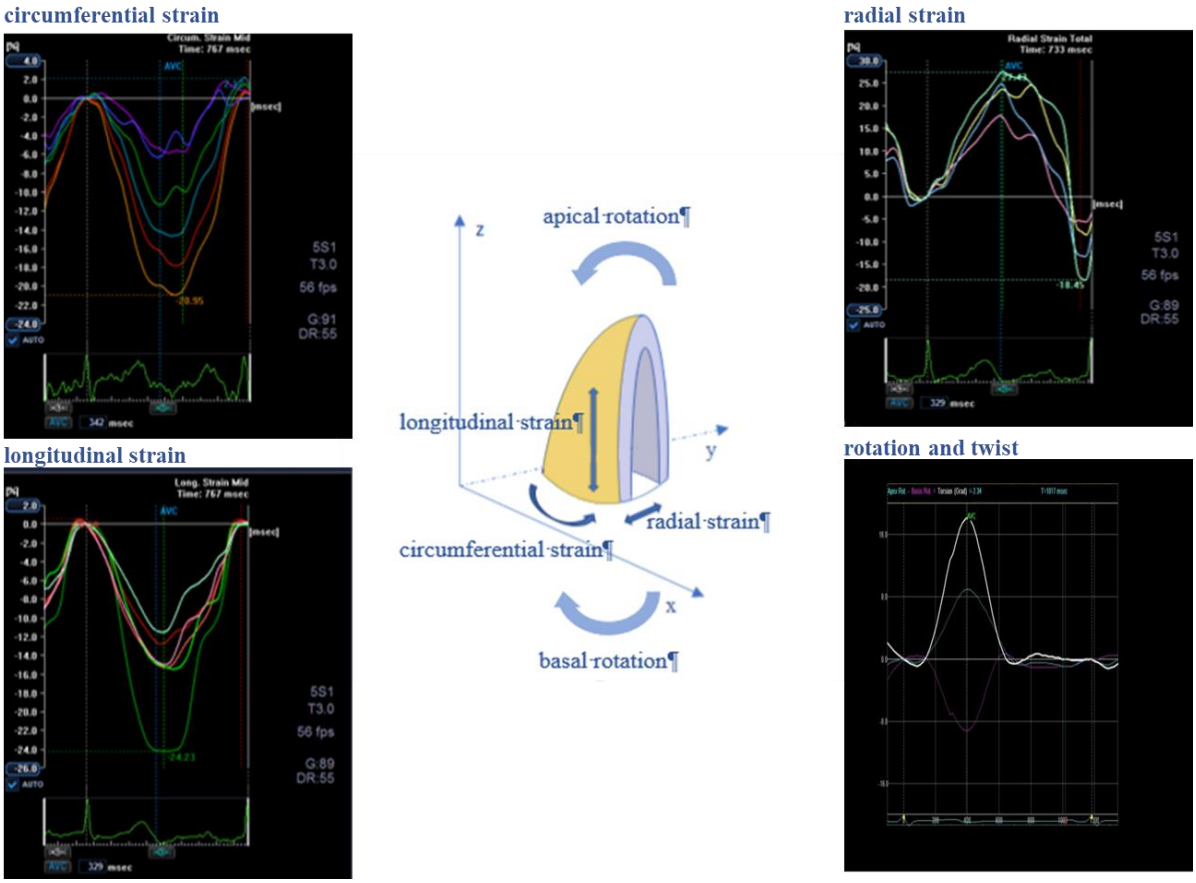

Figure 5. ***Components of myocardial deformation*** The **middle panel** shows the 3 normal strains (longitudinal, circumferential, and radial), oriented along the axes of the left ventricle. The **right and left panels** show typical strain curves of the respective component. The **lower right panel** shows rotation, defined by the view from the left ventricular apex to the base. The negative apical-basal rotation indicates the left ventricular twist. **Dashed green lines** represent the aortic valve closure.

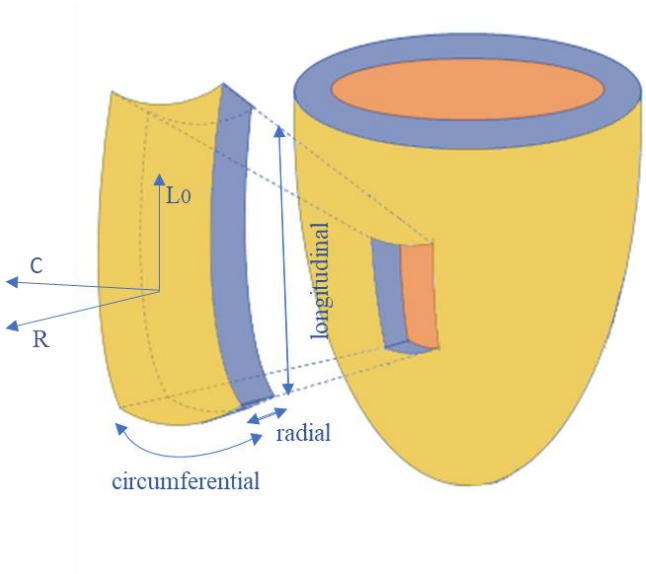

Figure 6. ***Longitudinal, radial and circumferential strain in the left ventricle***
Lo-longitudinal, C-circumferential and R-radial strain.

The spatial integral of circumferential–longitudinal shear strain from base to apex is identical to the global ventricular torsion. During the 3-dimensional movement of the left ventricle, systolic twisting and diastolic untwisting are created. It should be distinguished from the global and regional (segmental) strains. The global strain is the mean of the segmental strain values. Deformation imaging measurements correspond to cardiac function [9]. Considering the techniques of strain measurements, tissue Doppler imaging (TDI) uses one dimension, while speckle tracking two or three dimensions.

1.3.1 Tissue Doppler imaging

Tissue Doppler imaging (TDI) is used to measure the velocity of myocardial tissue, and it evaluates the essential parameters of myocardial deformation (strain and strain rate). This imaging technique is based on the Doppler effect, and enables the quantification of velocity in all heart segments during cardiac cycle. The calculated velocity can be displayed in two ways: as a pulsatile wave spectrogram or a colour coded image [8]. Using the latter, the movement towards the transducer is shown in red, while the movement away from it is expressed in blue. Higher speeds of movement are indicated by lighter colours. Due to the complicated movement, evoked by the anatomical orientation of the muscle fibres, the velocities measured by Doppler are very heterogeneous in the different myocardial segments. During contraction of the left

ventricle, the segments move towards the centre of gravity of the left ventricle (located at the upper third of the heart near the apex, perpendicular to the line of the atrioventricular valves, and directed towards the apex) [10]. Colour TDI mode has a frame rate of up to 200 frames per second (fps). It has the advantage of better temporal resolution and it can evaluate multiple structures and segments in a single view. The disadvantage of the method is angle dependence, which means that only deformations along the ultrasound beam can be calculated from velocities. The measurement is influenced by the translation and rotation of the heart, as well as the tethering of nearby segments.

1.3.2 Speckle tracking

The term "speckle" is used to describe the grey scale ultrasound pattern of the heart muscle. This unique pattern is created by the interference of ultrasound beams due to their spreading across the fine structures of the myocardium. Speckles arise as a consequence of reflections, and they correlate to the morphologic entities of the myocardial tissue but they are also influenced by ultrasound wave interactions. The speckle pattern of a myocardial segment ("kernel") is captured and stored by the software as a natural acoustic marker. The speckle patterns are identified frame by frame in the region of interest (ROI) called tracking area so the deformation of the myocardium can be automatically tracked during the cardiac cycle. After several frames, some speckles may change as some of them will get out of plane, while others enter the plane, but the kernel remains traceable. The traceability is based on a mathematical algorithm called sum of absolute differences (SAD). It allows the identification of the new position, which is the area of the lowest SAD value within that region. With a frame rate of 40-60 fps, correct assessments can be achieved in 2D speckle tracking. The limitation of this technique is that it requires excellent image quality [11]. The proper detection of endocardial and epicardial borders is essential, and if it is necessary, manual adjustments should be made. Exclusively tracking the subendocardial layers results in lower global strain values, compared to tracking the complete ventricular wall using medium or wide tracking area widths [12]. The size of the left ventricle also influences the measurement as it is usually difficult to view the entire myocardium, especially its apical segments in an enlarged left ventricle.

Finally, the speckles have a complicated motion in the 3D space, therefore speckle tracking measurements are sometimes challenging due to the motion of speckles beyond the plane, provoked by the motion of the heart during cardiac cycle [13]. This inadequacy can be corrected

by the 3D speckle tracking method. The development of ultrasound transducer technology has made possible almost real-time 3D imaging of the left ventricle (LV) with satisfactory image quality and temporal resolution. The analysis of the 3D data set starts with the automatic generation of a cube-shaped ROI. The 3DSTE algorithm evaluates the quality, and filters presumed artefacts (outliers). The disadvantage of this method is that it assumes a regular heart rhythm, and requires good respiratory cooperation to avoid artefacts. The optimal frame rate is between 35 and 50 fps. The results are mapped into an average myocardial mesh. Finally, the quantitative results of LV deformation are derived from this mesh model [14].

1.3.3 Standardisation of deformation imaging

One of the fastest growing branches of echocardiography is deformation imaging. It is used in the diagnosis of a wide range of heart diseases. However, several investigators have documented a relatively poor reproducibility when strain is calculated using echocardiographic equipment of different vendors. This problem interferes with the widespread clinical application of this important new technology.

Recognising the critical need for standardisation in strain imaging, in 2010 the leaders of the European Association of Echocardiography (now the European Association of Cardiovascular Imaging, EACVI), and the American Society of Echocardiography (ASE) invited the technical representatives of all the interested vendors to make a mutual effort to reduce intervendor variability of strain measurements [15]. A few years later, the comparison of global longitudinal strain, measured by the echocardiographic instruments of nine different vendors, showed that the reproducibility of global longitudinal strain (GLS) measurements was appropriate, and in many cases it was better than conventional echocardiographic assessments [16]. The consensus document for the standardization of deformation imaging was published in 2015 [17].

1.3.4 Foreshortening

An excellent image quality with the adequate representation of the respective sectional planes of the heart is required for proper image analysis. A main problem in clinical practice is the foreshortening of the apical views. Foreshortening means the scanning of oblique longitudinal views representing shortened left ventricular (LV) segments. It occurs when the operator places

the transducer in a suboptimal – mostly too cranial and too medial – position to get a presumably better view of the heart, which does not correspond to the apical standardised view.

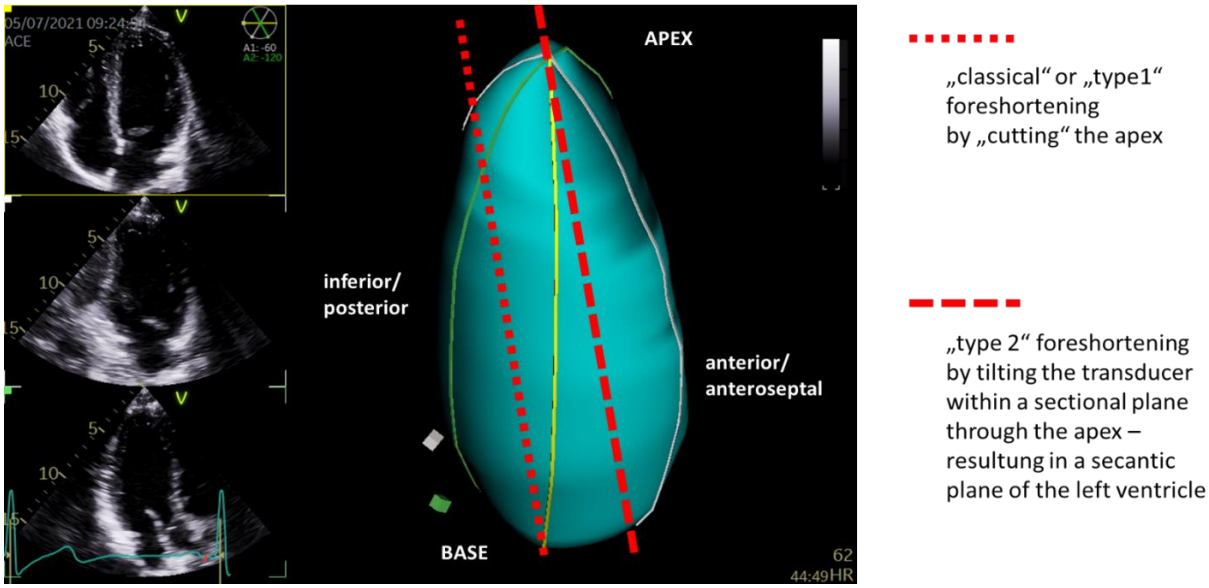

Figure 7. ***Visualization of foreshortening*** In the four-chamber view the yellow line shows the proper view. The red lines show the two types of foreshortening.

The foreshortening of apical views can occur in two ways: (1) The transducer is not placed at the apex of the heart but one or two ribs above the proper place. As a result, the myocardium becomes thicker at the apex and the LV long axis becomes shorter. (2) If the transducer is placed exactly at the apex but tilted caudally, the heart base appears closer to the “foreshortened” apex (Figure 6). This has an effect on the measurements of both conventional and deformation imaging echocardiography [18]. For this reason, a specific algorithm has been developed to prevent and detect apical foreshortening [19].

1.4 Cardiotoxicity

Over the past decade, the early detection of malignancies and the rapid development of oncological therapies have led to a significant improvement in cancer survival, but at the same time, a marked increase in mortality has been observed in cancer survivors due to cardiovascular diseases [20]. Cardiovascular disorders may develop from the beginning of chemotherapeutic treatment through the whole course of the malignant disease and are a potential complication of oncotherapy.

1.4.1 The intrinsic effects of tumours on the heart

Tumours can have several effects on the cardiovascular system. In 2014 Cramer *et al.* showed that patients with colorectal carcinoma, even though not treated with chemotherapy, have significantly reduced left ventricular function, decreased exercise capacity, lean mass, and heart rate variability, compared to healthy controls [21]. Patients with a malignancy often have an increased resting heart rate. This is however not influenced by the fact whether chemotherapy or potentially cardiotoxic chemotherapy was given previously. The resting heart rate is an independent predictor of survival as ≥75 beats per minute is associated with a worse outcome [22]. The increased heart rate may represent the activation of the sympathetic nervous system. Low heart rate variability also indicates the effect of the malignancy on the function of the autonomic nervous system. The more advanced the cancer, the lower the heart rate variability [14, 23, 24]. Tumour induced cachexia, which might develop in advanced stages, is not only associated with a reduction on the working muscle mass, but also a loss of myocardial mass. This condition may lead to heart failure, which further aggravates the course of the malignant disease and results in poor prognosis. Understanding the exact pathophysiological effect of malignancies on the heart still remains a challenge, which might be explained by the fact that different cancers are diverse regarding their pathomechanisms.

1.4.1.1 Chronic inflammation

The balance of energy use and production, known as metabolism, ensures proper functioning of the myocardium. Cardiac metabolism may be impaired by chronic inflammation and oxidative stress [25] leading to heart failure later.

A correlation between elevated interleukin 6 (IL-6) levels and the acute dysfunction of the heart has been already described [26]. Chronic elevation of proinflammatory cytokines such as IL-6 leads to a change in the metabolism of the heart, which may finally result in myocardial dysfunction. It has been suggested that IL-6 promotes the induction of fetal genes such as MyHCβ, and the reactivation of the fetal gene pattern and the subsequent isoform switch from adult MyHCβ to fetal MyHCα are associated with heart failure [27]. Another mediator of the inflammatory response is TNF-α, a potent activator of muscle-specific RING-finger protein-1 (MuRF1) and E3-ligase, which are involved in protein degradation. MuRF1 participates in the degradation of creatine kinase, thereby affecting energy metabolism [28]. MuRF1 targets

structural proteins such as MyHC or troponin I. MuRF1 transgenic mice have decreased LV wall thickness, while MuRF1 knock-out mice are protected against glucocorticoid induced cardiac atrophy [29]. Other crucial factors include the E3 ligase and the cachexokines. The first one is required for proteasomal degradation and is involved in the targeting of proteins. These labelled, i.e., polyubiquitinylated proteins, are then hydrolysed by the 26S proteasome. This mechanism promotes muscle atrophy as well [25]. Cachexokines (e.g., Ataxin-10) are tumour secreted factors, which have been isolated from cancer patients. These factors can induce cardiac atrophy and aberrant fatty acid metabolism in cardiomyocytes [30].

1.4.1.2 Oxidative stress

Besides inflammation, dysfunction of the respiratory chain can also lead to increased oxidative stress. Reactive oxygen species (ROS) are produced as metabolic byproducts of biological systems in different cellular compartments. In cardiomyocytes ROS typically originates from various intracellular sources including mitochondria. Enzymes such as nitric oxide synthase (NOS), xanthine oxidase, NADPH oxidase and cytochrome P450 are involved in their production. The major part of ROS is produced in the mitochondria. These ROS are mainly generated in the electron transport chain of the inner mitochondrial membrane during the process of oxidative phosphorylation. In advanced stages of malignancies, tumour induced cardiac cachexia also leads to ROS overproduction. In addition, leukocytes infiltrating the myocardial tissue are responsible for the development of the majority of ROS and reactive nitrogen species (RNS) through the production of superoxide and the release of prooxidant enzymes such as myeloperoxidase (MPO). ROS can alter calcium homeostasis by stimulating calcium release and inhibiting calcium reuptake in the sarcoplasmic reticulum resulting in calcium overload [31], which then contributes to impaired contractile function by stimulating the liberation of the proapoptotic factor cytochrome c [25].

1.4.2 The effect of various chemotherapeutic agents on the heart

Before and during chemotherapy, the balance of the beneficial effects and side effects of the specific drugs must be regularly evaluated. Cardiotoxicity is a major side effect of chemotherapy in oncological patients. According to the National Cancer Institute of the United States, it is defined as a toxicity that affects the heart. This process leads to changes not only in

resting cardiac parameters, but also in dynamic cardiovascular assessments during follow-up. Some of the most serious side effects are ventricular dysfunction and subsequent heart failure. The aim of the oncological treatment is to selectively destroy tumour cells and/or prevent tumour cell proliferation. At the molecular level, the therapy therefore targets the regions necessary for cell division and survival including DNA, mitotic spindle, mitochondria, proteosomes, certain kinases, and tumour-specific antigens, thus oncological therapies may lead to cardiotoxicity through various molecular mechanisms.

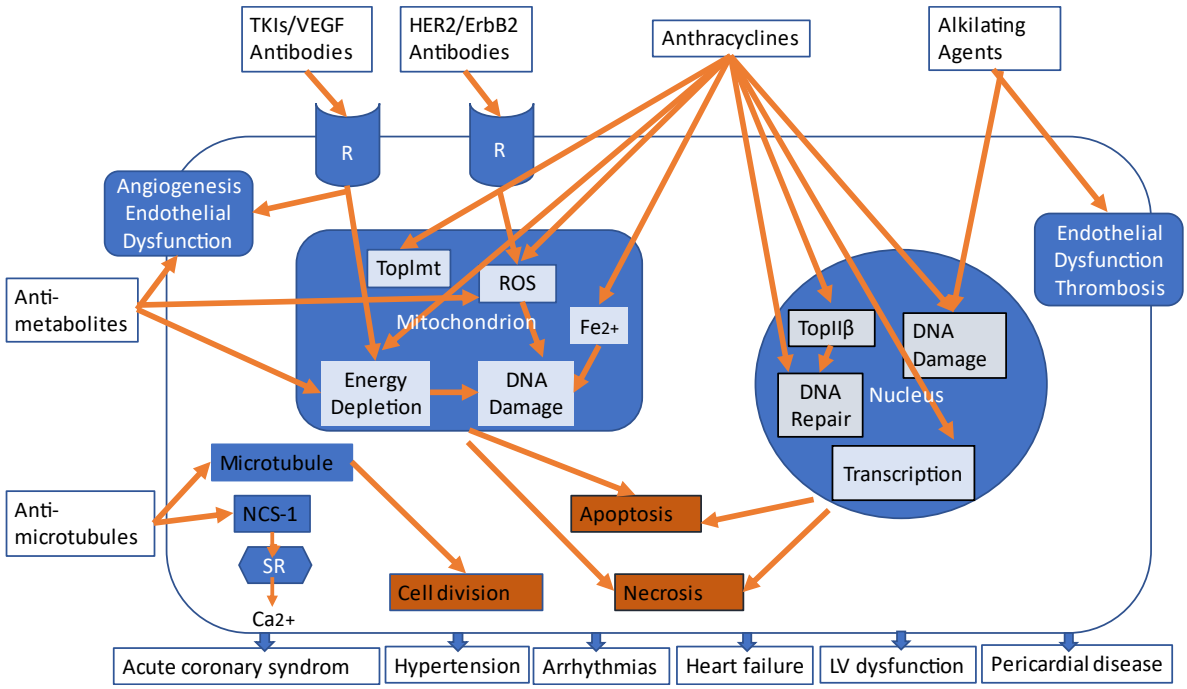

Figure 8. ***The effect of various chemotherapies on myocardial cells according to Han et al.*** [32]

1.4.2.1 Anthracyclines

Anthracyclines are commonly used cytostatic agents in the treatment of the acute stages of leukaemias and solid tumours. The exact mechanism of anthracycline-induced cardiomyopathy is unclear but there are many theories such as the inhibition of DNA replication and RNA transcription, the generation of free radicals leading to DNA damage or lipid peroxidation, DNA alkylation, DNA cross-linking, inhibition of DNA strand unwinding and helicase activity, direct membrane damage caused by lipid oxidation, and blocking of topoisomerase II.

The three main cell damage pathways are the following:

- disruption of DNA and RNA synthesis (intercalation)
- DNA strand breaks evoked by the inhibition of topoisomerase II
- activation of proapoptotic signalling pathways.

In accordance with this, anthracyclines exert toxic effects on three cellular components: mitochondria, cytosol, and cell nucleus. The most used agents are doxorubicin, daunorubicin, epirubicin, idarubicin and mitoxantrone.

Doxorubicin can bind to cardiolipin, a membrane-bound mitochondrial protein, causing direct mitochondrial damage. In addition, doxorubicin results in altered mitochondrial gene expression and the formation of intramitochondrial superoxides, which ultimately results in cell organelle death through increased mitophagy [33]. The additional negative effects arise due to altered mitochondrial iron transport and the activation of the proapoptotic regulator and tumour suppressor p53. Finally, the mitochondrial redox response is directly impaired leading to an increase in ROS [34].

In a group of 1230 patients with cardiomyopathy with a median follow-up of 4.4 years, Felker *et al.* have shown that doxorubicin-induced cardiomyopathy is associated with a poor prognosis [35]. LV dysfunction during anthracycline treatment may result in the manifestation of heart failure and is associated with increased mortality. The highest incidence of cardiotoxicity after anthracycline-based therapies has been observed during the first year [36].

Cardiotoxicity depends on the following:

- other risk factors of the patient,
- cumulative dose of anthracyclines,
- maximal single dose of anthracyclines,
- concomitant thoracic irradiation and HER2 inhibitor therapy [37].

1.4.2.2 Therapies with antibodies against human epidermal growth factor receptor-2

The catalytic activity of human epidermal growth factor receptor-2 (HER2) is essential for the development of the heart. Antibodies against HER2 are often used in combination with or after anthracycline-based treatments. The sole toxicity of HER2-based therapies has not been clearly demonstrated by clinical data [38]. Persistent genetic deletion of HER2 in adult myocardial cells leads to dilated cardiomyopathy with reduced LV function and thinning of the heart walls [39]. Calcium handling and mitochondrial function are influenced by a HER2-mediated

signalling cascade, triggered by the activation of mitogen-activated protein kinase (MAP) kinases [34].

1.4.2.3 Alkylating agents

Alkylating agents are the oldest class of drugs used in oncotherapy. They include nitrogen mustard (i.e., cyclophosphamide and ifosfamide) and the platinum-containing molecule, cisplatin. They act by binding to negatively charged DNA regions, causing strand breaks and cross-linking. Cyclophosphamide is a prodrug that – when activated – forms an alkylating molecule, which can bind to the DNA. Manifestations of cyclophosphamide-induced cardiotoxicity include pericarditis, myocarditis, and heart failure with irreversible damages in a high percentage of patients at higher doses. In accordance with this, high dose cyclophosphamide has been associated with non-cumulative incidence of heart failure, seen in up to 30% of patients shortly after the initiation of chemotherapy [40].

Cisplatin is used to treat different types of tumours (sarcomas, carcinomas [e.g., small cell lung cancer, ovarian cancer], lymphomas and germ cell tumours). It has acute and cumulative cardiotoxicity including ECG abnormalities, angina, acute myocardial infarction, hypertension, hypotension, arrhythmias, myocarditis, cardiomyopathy, and congestive heart failure [41]. Cisplatin-induced cardiac dysfunction is associated with mitochondrial membrane depolarisation and ultrastructural alterations (mitochondrial DNA damage). Following cisplatin treatment, cardiomyocytes show mitochondrial abnormalities such as mitochondrial membrane depolarisation, inflammatory responses and increased endoplasmic reticulum stress resulting in the stimulation of caspase-3 activity [42]. In addition, a correlation between oxidative stress and cisplatin-induced cardiomyocyte apoptosis has been demonstrated. Nuclear DNA damage has also been observed [43]. Moreover, the platinum-based therapies increase the risk of thrombotic events. This can be explained by the fact that platinum induces platelet activation and aggregation, as well as the alteration of the endothelial cell integrity.

1.4.2.4 Proteasome Inhibitors

Proteasome inhibitors are used in the treatment of multiple myeloma exerting their effects through the reversible (e.g., bortezomib) or irreversible (e.g., carfilzomib) inhibition of the proteosome. As cardiomyocytes do not proliferate and they have elevated proteasome activity,

compared to other tissues, they are particularly sensitive to proteosome inhibition. Carfilzomib is most significantly associated with cardiotoxicity among these chemotherapeutic agents as it irreversibly blocks the 20S subunit of the proteasome. This inhibition is assumed to play a role in the development of the deterioration of left ventricular function [44].

1.4.2.5 Tyrosine kinase inhibitors

Tyrosine kinase inhibitors are a large group of drugs that play a prominent role in the treatment of various malignancies, and depending on their molecular targets, are associated with specific cardiovascular complications. Their main targets are the vascular endothelial growth factor (VEGF) receptors. VEGF includes several proteins that have a function in angiogenesis by controlling proliferation and endothelial cell growth. VEGF proteins are also essential for normal cardiac development and responsible for the structural integrity of the adult heart. There is also evidence of increased damage on the cardiac mitochondria and the generation of ROS due to tyrosine kinase inhibitors [45]. Their most common side effect is a usually transient impairment of left ventricular function. Furthermore, the use of tyrosine kinase inhibitors is associated with the occurrence of atrial fibrillation and other cardiac arrhythmias [46]. After chronic exposure to ibrutinib, the inhibition of phosphoinositide 3-kinase results in an increased late sodium current, which may lead to the prolongation of cardiac action potential and subsequently to a higher susceptibility to early and delayed after-depolarisation elevating the risk of both atrial and ventricular arrhythmias [47].

1.4.2.6 BRAF and MEK inhibitors

The antiproliferative effect of these drugs is based on the inhibition of the MAP kinase signalling pathway. This type of treatment is mainly used in advanced malignant melanomas because mutations in this signalling pathway are common in this stage of the disease and cause an uncontrolled proliferation. Kinases that are part of this signalling pathway are involved in cardiomyocyte hypertrophy, myocardial development, and apoptosis as well [48]. Pharmacological inhibition of the MAP pathway can lead to a reduction in left ventricular function at the beginning of treatment.

1.4.2.7 Antimetabolites (fluoropyrimidines)

Fluoropyrimidines are the second most common cause of cardiotoxicity, the exact mechanism of which remains unclear. Coronary vasospasm and endothelial injury are the main cardiovascular implications of these antimetabolites. Thyss *et al.* have found elevated plasma levels of endothelin-1 in patients with 5-fluorouracil-induced (5-FU) cardiotoxicity. Increased endothelin-1 levels lead to coronary vasospasm and ischemia [49], and experimental studies have demonstrated an effect of direct myocardial toxicity as well [50]. An extensive literature review has shown that 5-FU can induce apoptosis and apophagy in cardiomyocytes and endothelial cells via the production of oxidative stress. Saif *et al.* have reported that angina occurred in 45% of patients with 5-FU-associated cardiotoxicity, whereas myocardial infarction was seen in 22%, arrhythmias in 23%, acute pulmonary oedema in 5%, cardiac arrest and pericarditis in 1.4% and heart failure in 2% of cases [51].

1.4.2.8 Immune checkpoint inhibitors

Immune checkpoint inhibitors are a new class of anti-cancer drugs, distinct from targeted or tumour-type-specific therapies. According to their mechanism of action, these agents are monoclonal antibodies directed against immune checkpoints, namely cytotoxic T lymphocyte-associated antigen 4 (CTLA-4), programmed cell death 1 (PD-1) and its ligand 1 (PD-L1). They help to restore the anti-tumour activity of cytotoxic T-lymphocytes, thereby triggering anti-cancer immunity. In addition to this intended cytotoxic reaction, they can lead to an unwanted immune reaction against myocardial tissues. A direct invasion of activated T cells into the myocardium, or an indirect immune reaction with the development of autoantibodies against cardiac troponin I have been described [52]. In the recent years, numerous cases of pericarditis, myocarditis and fatal heart failure have been reported in patients treated with checkpoint inhibitors. Immune checkpoint inhibitor-related myocarditis usually occurs within the first 6 weeks of therapy [53], and is the most lethal type of immune-related adverse event with a mortality rate of 27-46% [52, 53].

Because of the potential cardiotoxic effects described above, it is important to detect cardiac damage as early as possible since it allows the reconsideration of therapy and timely initiation of cardioprotective treatment. Oncocardiology aims to enhance diagnosis and improve the treatment of cardiovascular diseases caused by cancer therapy. Identifying the group of patients

at risk and detecting cardiotoxicity in time remain a challenge. The CARDIOTOX registry, published in 2020, was a prospective multicentre study with a large cohort of 1324 patients, designed to identify cardiovascular risk factors associated with cancer therapy, to evaluate the utility of clinical, biochemical and ECHO parameters in the early detection of cardiovascular diseases in patients treated with cancer therapy, and to assess potential factors associated with the prognosis and recovery of LV function [54]. The risk of left ventricular dysfunction varies from <1% (paclitaxel) to 48% (high-dose doxorubicin therapy with 700mg/m^2 dose) [55].

1.4.3 Biomarkers

Biomarkers are an essential component of the diagnosis of acute and chronic heart diseases. In addition to their role in the early detection of cardiovascular disorders, they are also important in monitoring cardioprotective treatment responses.

According to the European guideline, the NT-Pro BNP and BNP are the classic biomarkers of heart failure and the occurrence of atrial fibrillation. Both markers have high sensitivity and low specificity [56]. The NT-Pro BNP/BNP level is influenced by renal function, age, diabetes mellitus, arterial hypertension, atrial fibrillation, and gender. In cancer patients anaemia and fluid imbalance may have also an effect on the value of these biomarkers [57].

Troponin I and troponin T are characteristic biomarkers of myocardial injury and thus may be elevated not only in myocardial infarction but also in other cardiovascular and pulmonary diseases, and are associated with increased all-cause mortality [58–60]. The development of high-sensitivity cardiac troponin (hs-cTn) assays has made it possible to accurately quantify low concentrations. Measurement of these laboratory parameters prior to the initiation of therapy is recommended, and the timing and frequency of biomarker assessments should be adjusted to the specific biomarker-chemotherapy combination. Based on the recommendations of the ESC, different survival protocols have been developed according to the baseline cardiac risk and the chemotherapy of choice [60].

1.4.4 The role of echocardiography

In addition to biomarkers, the significance of cardiac imaging has changed in recent years. The commonly used imaging parameter to detect cardiotoxicity was LV ejection fraction (LVEF) in former years.

Endomyocardial biopsy analysis has been found to be the most sensitive and specific method to identify cardiomyopathies of different origin after detection of LV dysfunction. Cardiomyopathies attributed to anthracyclines was mostly identified by biopsies and this technique was the gold standard in the 1970s. Its major disadvantage is invasiveness. Due to this, there was a need to develop non-invasive methods for the detection of myocardial damage. Echocardiography is a widely used technique with the advantage of easy access, repetitive follow-ups, and multimodality, and it is safe for people with concomitant kidney disease without the hazard of x-ray exposure. cardiac magnetic resonance (CMR) is a useful complementary method to echocardiography, especially in cases of limited echo quality. With the help of this, a reliable ejection fraction and better tissue characterisation can be obtained, and edema, strain, diffuse and focal fibrosis can be assessed as well. Late gadolinium enhancement (LGE) is a reliable method for the detection of myocardial fibrosis. There is a correlation between 2D longitudinal segmental strain and LGE areas when using CMR [61].

Cancer therapy-associated cardiac dysfunction is defined as a decrease in LVEF below 50% or by >10% from baseline to a value below the lower limit of normal (53%); it is also considered when the global longitudinal strain (GLS) falls below -18% or shows a >15% relative reduction to a value below the normal range (0% to -17.9%) [37].

A recent prospective, randomised, controlled trial of 331 anthracycline-treated participants has shown that the GLS-controlled arm had a significantly lower reduction in LVEF at 1-year follow-up, compared to the LVEF-controlled group. Furthermore, the GLS-guided cardioprotective therapy significantly prevented the decline of LVEF into the abnormal range. These results support the application of GLS in the monitoring of cancer therapy-related cardiac dysfunction [62].

2 Aims

I. To investigate strain patterns and cardiotoxicity using standardised new echocardiographic methods.

The first study was designed to underline the importance of standardisation in echocardiography.

II. To evaluate the effect of foreshortening on the quantitative parameters of tissue Doppler and 2D speckle tracking.

Considering that chemotherapy-associated cardiac dysfunction may result in an increased mortality, early detection of specific echocardiographic parameters, and thus, the modification of chemotherapy and/or the initiation of cardioprotective treatment may improve survival. Therefore, the aim of the second study was:

III. To determine whether early cardiac manifestations in patients receiving chemotherapy can be detected by standardised 2D and 3D echocardiography using conventional and deformation parameters.

3 Materials and methods

In our study evaluating the impact of foreshortening, 54 patients with normal wall motion pattern and normal ejection fraction (EF 65.5±6.8%) were enrolled in the Department of Cardiology and Angiology, University of Leipzig, Leipzig, Germany from April 2011 to June 2011. All patients had sinus rhythm and optimal acoustic window using the apical transthoracic approach during the echocardiographic examination. Patients whose heart segments were not clearly visible throughout the whole cardiac cycle were excluded from the study. The study group consisted of 32 men and 22 women with a mean age of 49±17 years (range 23 to 83 years). Forty-six percent of them had hypertensive heart disease, while the rest of them had no signs of any kind of heart disorder. All study subjects were provided informed consent after the full explanation of the purpose and nature of the study. All procedures were approved by the local ethics committee.

In our other study evaluating the early detection of cardiotoxicity, two groups involving 25-25 study subjects (n=50) were enrolled from November 2012 to April 2013 in the aforementioned cardiology department. All study subjects were provided informed consent after the full explanation of the purpose and nature of the study. All procedures were approved by the local ethics committee. Subjects with LVEF<30% before chemotherapy and accompanying diseases such as cardiac arrhythmias, mild or severe valvular stenoses or regurgitations, prosthetic valves or pacemaker were excluded. It should be underlined, that only subjects with excellent image quality were included in the study. The excellent image quality enables reliable tracking of the myocardial speckles and thus good tracking curves. In group 1 twenty-five healthy subjects (controls) without any cardiovascular diseases or cardiovascular risk factors were analysed. In group 2 twenty-five patients with various malignancies undergoing several types of cardiotoxic chemotherapies were investigated before and during chemotherapy for a mean follow-up of 3 months (±2 weeks). Clinical data of all controls (group 1) and patients (group 2) are shown in Table 1.

Clinical data	Group 1 (n=25)	Group 2 (n=25)	p value
Age (years)	45±12	63±15	0.37
Male	16 (64%)	11 (44%)	0.13
Female	9 (36%)	14 (56%)	0.13
Smoker	6 (24%)	7 (28%)	0.71
Alcohol consumption	0 (0%)	0 (0%)	NS
Arterial hypertension	5 (20%)	11 (44%)	0.41
Coronary heart disease	0 (0%)	2 (8%)	0.15
Pulmonary embolism	0 (0%)	1 (4%)	0.31
Type 2 diabetes mellitus	0 (0%)	5 (20%)	0.16
Peripheral arterial disease	0 (0%)	2 (8%)	0.15
Hypercholesterinemia	0 (0%)	2 (8%)	0.15
Chronic obstructive pulmonary disease	0 (0%)	4 (16%)	0.34
β-blocker therapy	10 (40%)	7 (28%)	0.29
ACE-inhibitor therapy	11 (44%)	5 (20%)	0.29
Calcium antagonist therapy	0 (0%)	2 (8%)	0.15

Table 1. ***Clinical data of controls and patients***

The various tumour types included in the study were acute myeloid leukaemia (1 patient), B-cell non-Hodgkin lymphoma (1 patient), multiple myeloma (2 patient), breast (10 patient), stomach (4 patient), lung (2 patient), thyroid (1 patient) and lingual (2 patient) cancer, hepatocellular (1 patient) and renal cell carcinoma (1 patient). Chemotherapy was performed with the use of anthracycline (n=7), platinum-based antineoplastic agents (n=4), taxoids (n=5), paclitaxel (n=1), monoclonal antibodies (MABs) (n=6), kinase inhibitors (n=2), alkylating agents (n=3) and their combination (taxoid-anthracycline, MAB-anthracycline or MAB-platinum based antineoplastic agent).

3.1 Echocardiographic analysis of the study investigating the impact of foreshortening

Standard 2D and Doppler echocardiography were performed according to the guidelines of the European Association of Echocardiography and the American Society of Echocardiography [63, 64] using Vivid E9 system (GE Healthcare) with a 1.5-4.6 MHz matrix array transducer at a frame rate between 40 and 80 frames/sec. A defined five chamber view (5ChV) was acquired in addition to the standard four chamber view (4ChV) to demonstrate the foreshortening. The angle of foreshortening was measured by the diastolic diameter of the mitral annulus, and the diastolic and systolic length of the left ventricle applying the monoplane Simpson´s rule and the auto EF method [65]. View acquisition was repeated three times, and then stored in a cine loop format for offline analysis with EchoPAC software (version 110.1.1.) (Figure 9).

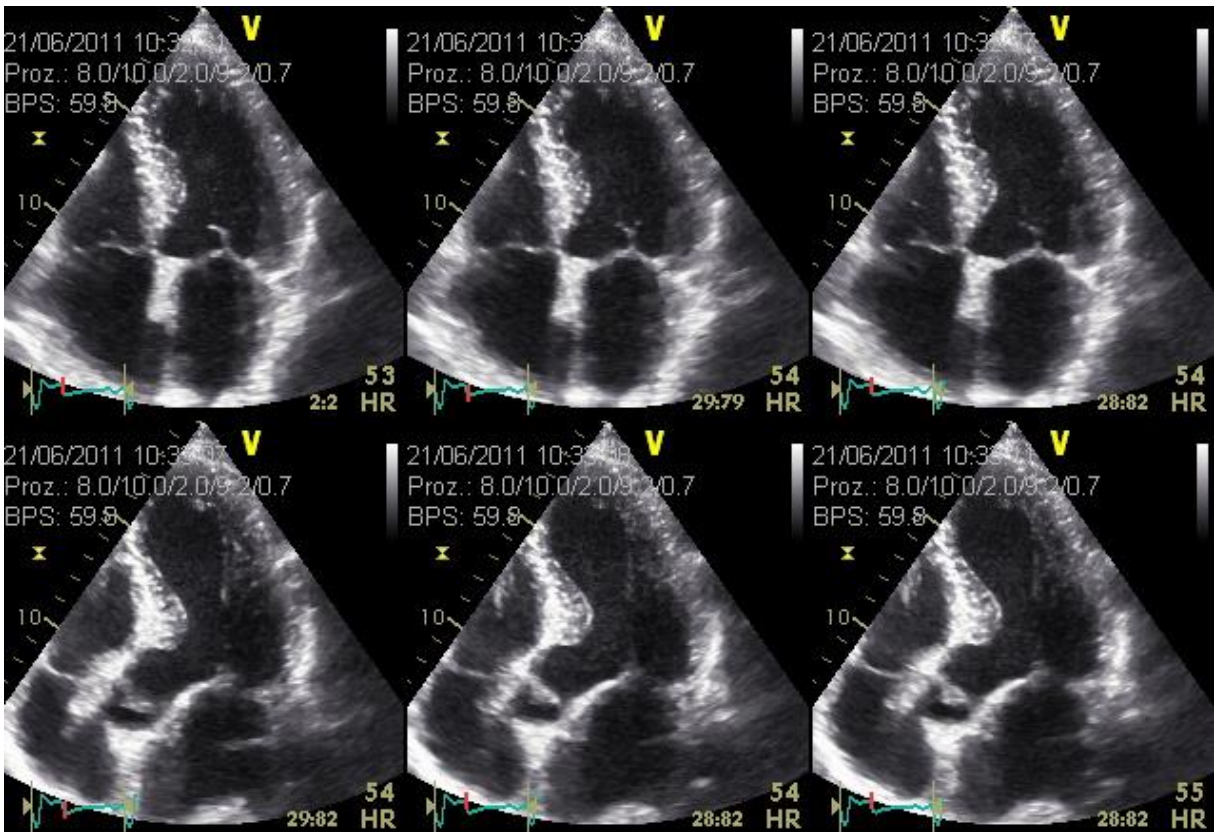

Figure 9. ***Three consecutive views (4ChV and 5ChV) to illustrate documentation modalities in the study***

Colour tissue velocity images were also used for the measurement of tissue velocity imaging (TVI)-based strain with a colour frame rate of 100–140 frames/sec. To test reproducibility, three cardiac cycles during breath-holding were saved in a digital format. Septal and lateral regional

peak systolic strains (PSS) of 2D longitudinal strain in monoplane 2D loops were analysed with speckle tracking by both views. PSS was also calculated from the TVI views to compare the results of strain measurements between both methods.

3.2 Echocardiographic methods to study the early detection of cardiotoxicity

All controls and patients underwent 2D and 3D transthoracic echocardiography according to the European and American guidelines using Toshiba Artida Medical System (Zoetermeer, The Netherlands) with PST-25SX 1 MHz to 4 MHz phased-array matrix probe for 3D image acquisition [63, 64]. LVEF, left ventricular end-diastolic volume (LVEDV), left ventricular end-systolic volume (LVESV), left ventricular muscle mass, global longitudinal strain (GLS), global radial strain (GRS), and global circumferential strain (GCS) were measured offline using the 16-segment model of 2D and 3D echocardiography. Two-dimensional parasternal short axis views were acquired at the level of the left ventricular apex, the papillary muscles, and the mitral valve for the measurement of global radial and circumferential strains by 2D speckle tracking (ST). Two-dimensional apical long axis, two- and four-chamber views were acquired for the assessment of GLS by 2D ST. Two-dimensional apical views were acquired at fixed sectional planes with differences of ~60° between each other. All 2D views were compared to the views of the triplane approach. In addition, rotation and twist were analysed by 3D ST. Rotation refers to the myocardial rotational displacement around the long axis of the left ventricle. The difference between the apex-to-base left ventricular rotation is defined as the net LV twist angle [66]. Peak strain was measured during the ejection time in patients with normal deformation patterns, and after aortic valve closure in patients with post-systolic peak strain. The time-to-peak interval describes the time interval between aortic valve opening and the maximum strain during systole. Longitudinal, radial and circumferential time-to-peak intervals were measured in all 3D data sets of all controls and patients. LVEF was measured with semiautomatic 3D wall motion tracking (Wall motion tracking software, Toshiba Medical Systems). According to the methodological prerequisite for 2D ST, the frame rate should be between 40 and 80 frames/sec. In the present data sets, the frame rate was between 30 and 60 fps, with mean values of 57±6 and 25±2 in 2D and 3D ST, respectively. The width of the tracking area was manually selected. In all controls and patients, full myocardial tracking was performed. In patients with mild to moderate left ventricular hypertrophy, tracking areas were

adjusted to the wall thickness to ensure full myocardial tracking. The end-systole was determined automatically by the software at the time of aortic valve closure.

4 Statistical analysis and reproducibility

4.1 Statistical analysis and reproducibility of the study investigating the impact of foreshortening

All data are presented as mean ±standard deviation and standard error of the mean. Comparisons between the 4ChV and the defined foreshortened 5ChV were performed using a paired sample t-test in both subgroups as the data showed a normal distribution. A p-value<0.05 was considered statistically significant. Agreement between the TVI and speckle tracking based strain imaging methods was assessed by Bland-Altman analysis. One investigator analysed the longitudinal regions by 10 randomly selected patients twice to determine the intra-observer variability. Two independent investigators evaluated the echocardiographic parameters in 12 randomly selected patients for inter-observer variability. The data were analysed using SPSS (version 17.0, SPSS Inc, Chicago, IL, USA) and MedCalc for Windows (8.1.1.0 release, Mariakerke, Belgium) statistical softwares.

4.2 Statistical analysis of the study evaluating the early detection of cardiotoxicity

Mean values and standard deviations were calculated. Comparisons between groups 1 and 2 were performed by independent sample t-test. In group 2 data obtained before and during chemotherapy were compared with the help of paired sample t-test. P-values <0.05 were considered statistically significant. Statistical analysis was carried out with SPSS software (version 17.0, SPSS, Inc.). In 10 randomly selected patients, 2D and 3D measurements were performed by another investigator twice within 5 weeks to determine intra-observer variability. In addition, in 10 randomly selected patients, 2D and 3D measurements were carried out by two independent investigators to assess inter-observer variability.

5 Results

5.1 Results of the study assessing the impact of foreshortening

The effect of non-standardisation and foreshortening on LV volume measurement is shown in Table 2. The defined foreshortened view was characterised by a diastolic LV length of 75±8 mm. In comparison, the LV length, determined by a standardised 4ChV, was 81±8 mm (p<0.001). The systolic LV length was 58±7 mm in the defined foreshortened view and

63±7 mm in the standardised 4ChV (p<0.001). The diastolic diameter of the mitral valve annulus changed significantly as well (29±4 mm vs. 16±4 mm; p<0.001). The EF was 66±7% and 69±8% (p=0.001), measured in the standardised 4ChV and foreshortened view, respectively. Cardiac output, stroke volume as well as systolic and diastolic volumes were underestimated by the foreshortened views (Table 2).

	4ChV X±SD	**5ChV X±SD**	**p value**
Ejection fraction (%)	65.53±6.75	68.90±7.82	<0.001
End systolic volume (mL)	35.45±13.17	24.78±12	<0.0001
End diastolic volume (mL)	97.61±25.71	78.32±25.05	<0.0001
Systolic length of LV (mm)	62.86±6.70	58.06±6.85	<0.0001
Diastolic length of LV (mm)	81.23±7.95	74.99±7.86	<0.0001
Diastolic diameter of the mitral valve annulus (mm)	29.3±3.85	16.3±3.88	<0.0001
Cardiac output (L/min)	4.86±2.15	3.83±1.37	=0.001
Stroke volume (mL)	62.92±15.96	54±16.13	<0.0001

Table 2. ***Significant alteration of the classical parameters of LV geometry and function due to foreshortening in a population with normal wall motion pattern*** All estimated parameter showed a significant difference between the standard and foreshortened view, LV=left ventricular.

Three hundred and twenty-four segments were analysed three times in the standardised 4ChV and in the defined foreshortened view. Six regions of interest were defined in all patients. Within these regions (basal, mid, and apical septal as well as the basal, mid and apical lateral segments) the longitudinal peak systolic strain was assessed in the standardised 4ChV and the defined foreshortened view with speckle tracking and TVI (Table 3, 4; Figure 10, 11).

Segments	PSS by 4ChV (%)	PSS by 5ChV (%)	p-value
septal basal	-17.03±1.61	-14.81±3.26	**<0.0001**
mid septal	-20.26±2.31	-19.71±3.5	0.097
septal apical	-25.52±4.74	-25.96±5.83	0.46
lateral basal	-19.6±3.28	-20.19±4.3	0.22.
mid lateral	-20.62±3.3	-20.91±4.37	0.56
lateral apical	-23.92±5.11	-24.12±7.52	0.83

Table 3. ***The change of regional PSS values (speckle tracking based strain)*** Significant lower PSS value was observed in the septal basal region in the foreshortened 5 ChV compared with standard 4 ChV using the speckle tracking analysis.

Segments	PSS by 4ChV (%)	PSS by 5ChV (%)	p-value
septal basal	-18.23±5.71	-16.96±6.72	0.27
mid septal	-20.82±6.34	-22.17±8.72	0.35
septal apical	-23.16±10.17	-22.0±9.61	0.34
lateral basal	-18.91±6.91	-19.42±6.71	0.62
mid lateral	-16.91±6.34	-17.43±5.81	0.57
lateral apical	-12.1±5.68	-12.58±5.37	0.51

Table 4. ***Changes in PSS values of the 4ChV (TVI based strain)*** Non-significant changes were observed using the TVI-method

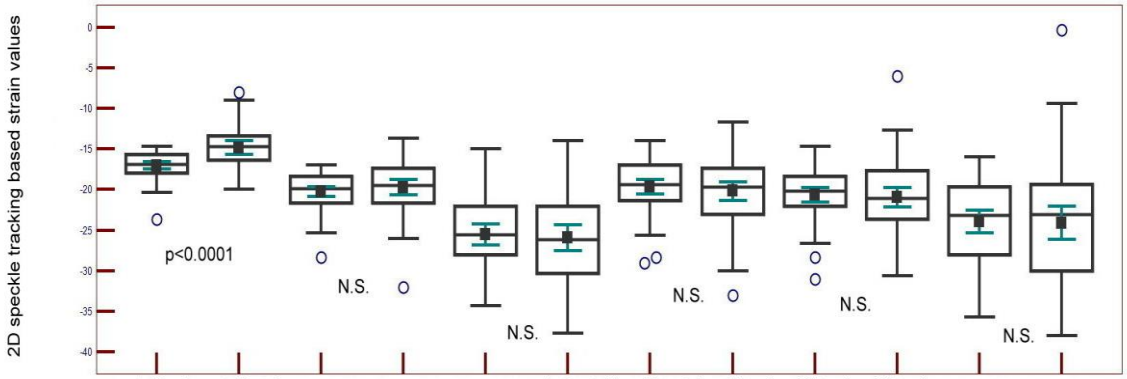

	septal basal 4ChV	septal basal 5ChV	mid septal 4ChV	mid septal 5ChV	apical septal 4ChV	apical septal 5ChV	basal lateral 4ChV	basal lateral 5ChV	mid lateral 4ChV	mid lateral 5ChV	apical lateral 4ChV	apical lateral 5ChV
Mean values of PSS	-17.03	-14.81	-20.26	-19.71	-25.52	-25.96	-19.6	-20.19	-20.62	-20.91	-23.92	-24.12
Standard deviation	1.61	3.26	2.31	3.5	4.74	5.83	3.28	4.3	3.3	4.37	5.11	7.52

Figure 10. ***2D speckle tracking based strain values, assessed in each region of the 4 and 5chV*** The basal septal PSS values significantly changed. PSS=peak systolic strain, 4ChV: 4 chamber view, 5ChV: 5 chamber view

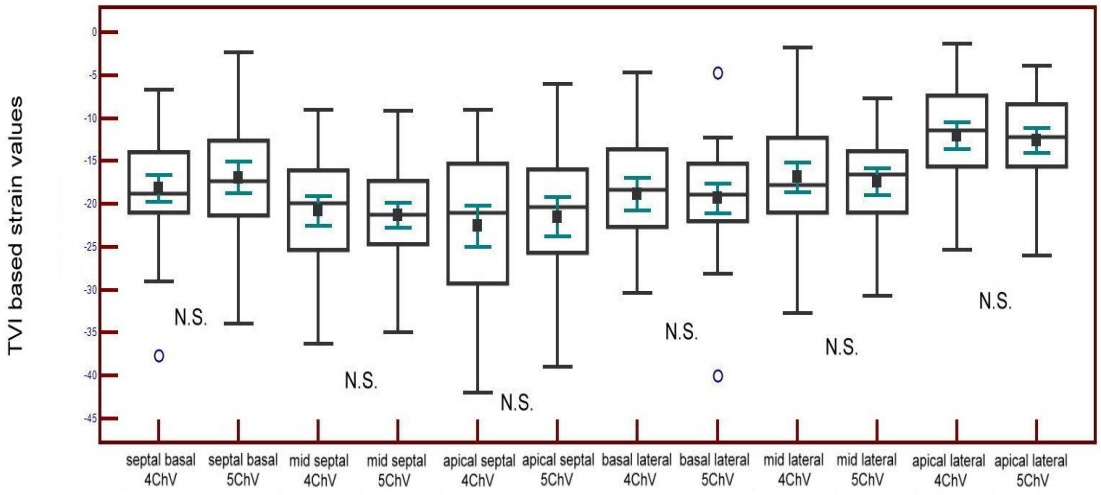

	septal basal 4ChV	septal basal 5ChV	mid septal 4ChV	mid septal 5ChV	apical septal 4ChV	apical septal 5ChV	basal lateral 4ChV	basal lateral 5ChV	mid lateral 4ChV	mid lateral 5ChV	apical lateral 4ChV	apical lateral 5ChV
Mean values of PSS	-18.23	-16.96	-20.82	-22.17	-23.16	-22	-18.91	-19.42	-16.91	-17.43	-12.1	-12.58
Standard deviation	5.71	6.72	6.34	8.72	10.17	9.61	6.91	6.71	6.34	5.81	5.68	5.37

Figure 11. ***The change of the mean TVI based PSS values due to foreshortening*** TVI: tissue velocity imaging, PSS: peak systolic strain. Non-significant changes were measured using the TVI-method

The parameters of regional strain, measured in the 4ChV, represented normal values in the cohort of patients with normal LV function. Although all 2D parameters showed a significant

change between 4ChV and the defined foreshortened view, there were only minor differences between the TVI and speckle tracking parameters. No statistical differences were obtained in the PSS parameters between the standard 4ChV and the defined foreshortened view, analysed by the tissue Doppler-derived method. However, the basal septal PSS, determined by 2D speckle tracking, was significantly lower in the defined foreshortened view than the standardised 4ChV. Correlation of longitudinal PSS values, determined by TVI and speckle tracking, showed an average difference of –2.98±8.55 and –2.52±9.35 (mean±SD) for the measurements in the 4ChV and the defined foreshortened view, respectively. The limits of agreement were 12.4 to –18.3 versus 15.2 to –20.2, respectively. Bland-Altman plots are depicted in Figure 12.

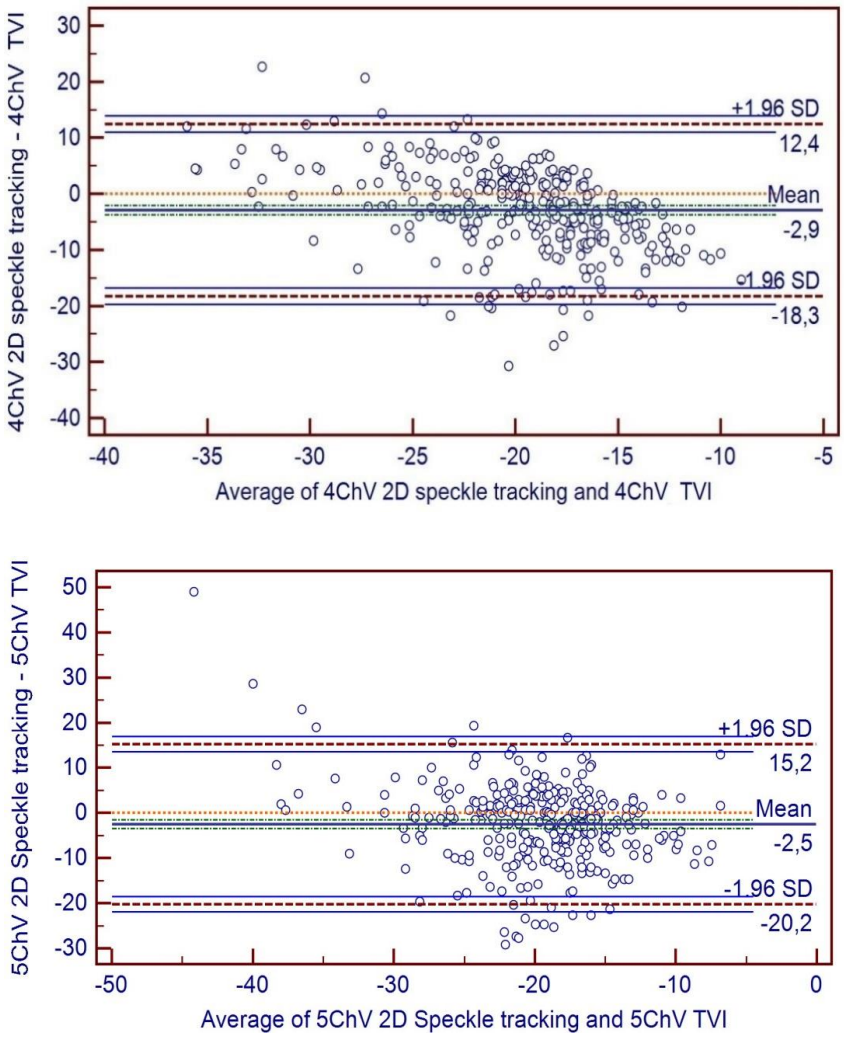

Figure 12. ***2D speckle tracking and TVI based measurements for the longitudinal strain in 4 ChV and 5 ChV*** Bland-Altman plots represent the disagreement between 2D speckle tracking

and TVI based measurements for longitudinal peak systolic strain in 4ChV and 5ChV. Red horizontal lines denote the bias (mean intermethod difference) and thick dotted horizontal lines depict the 95% limits of agreement.

There was no impact of foreshortening on the global PSS in patients with normal wall motion patterns (Table 5).

	4ChV	foreshortened view	p-value
global strain value ± SD (speckle tracking)	-21.9±3.1	-21,9±3.2	0,61 N.S.
global strain value ± SD (TVI)	-18.4±3	-18.4±3.6	0,84 N.S.

Table 5. ***Global strain values*** Non-significant changes in global strain values due to foreshortening.

Intra-observer and inter-observer variabilities of strain measurements were 4.6±1% and 4.7±1.8%, respectively.

5.2 Results of the study evaluating early detection of cardiotoxicity

Sixteen segments of 25 controls and 25 patients were tracked and analysed by 2D and 3D ST and 3D wall motion tracking. Conventional parameters are shown in Table 6. Compared to group 1, LVEF was reduced in group 2 at both time points (before and during chemotherapy). However, LVEF was not different in group 2 at the 3-month follow-up. For left ventricular volumes and left ventricular muscle mass, no significant differences were observed in the two study groups.

	Group 1	**Group 2 (before chemotherapy)**	**Group 2 (during chemotherapy)**
3D LVEF (%)	57±9	50±16^{*,a}	49±7^{*,b}
3D LVEDV (mL)	108±36	113±22	108±28
3D LVESV (mL)	47±25	56±14	55±16
3D muscle mass (g)	133±24	150±29	149±27

Table 6. ***Comparison of conventional parameters between groups 1 and 2 and between the two time points (group 2 before and during chemotherapy)*** *p-value <0.05, LVEF: left

ventricular ejection fraction, LVEDV: left ventricular end-diastolic volume, LVESV: left ventricular end-systolic volume.

[a] Comparison between groups 1 and 2 (before chemotherapy).

[b] Comparison between groups 1 and 2 (during chemotherapy).

In comparison to group 1, 2D GCS and 2D GLS were significantly higher at the 3-month follow-up, although there was no significant difference between group 1 and baseline group 2 data (before chemotherapy). However, for 2D radial strain, significant differences were observed between group 1 and baseline group 2 data (before chemotherapy), and between baseline and 3-month follow-up group 2 data (Table 6). 2D views and the corresponding strain curves are shown in Figures 12, 13, 14, 15, and 16. Values of 3D global circumferential strain were significantly higher in group 2 (both before and during chemotherapy) in comparison to group 1 (Table 7).

	Group 1	**Group 2 (before chemotherapy)**	**Group 2 (during chemotherapy)**
3D global radial strain (%)	34±16.67	28±12.75	26±14.48
3D global circumferential strain (%)	−28±1.71	−21±4.50*,a	−22±4.70*,b
3D global longitudinal strain (%)	−14±1.52	−13±2.55	−12±2.23
2D global radial strain (%)	23±9.38	28±10.56*,a	21±11.53*,c
2D global circumferential strain (%)	−23±3.77	−21±7.82	−18±8.21*,b
2D global longitudinal strain (%)	−16±2.90	−15±4.20	−14±4.56*,b
2D rotation (°)	1.3±0.27	1,02±0.24	0,82±0,18
3D rotation (°)	3.5±0.28	3.4±2.17	3.3±2.34
3D twist (°/cm)	3.5±2.24	4.2±2.68	4.4±2.88
3D time-to-peak interval (radial) (ms)	402±79.09	402±65.90	389±80.32
3D time-to-peak interval (circumferential) (ms)	359±70.17	382±45.03	380±76.74
3D time-to-peak interval (longitudinal) (ms)	375±68.28	379±55.09	355±65.71

Table 7. ***Comparison of deformation parameters between groups 1 and 2 and between the two time points (group 2 before and during chemotherapy)*** *p-value <0.05.

[a] Comparison between groups 1 and 2 (before chemotherapy).

[b] Comparison between groups 1 and 2 (during chemotherapy).

[c] Comparison between group 2 before and group 2 during chemotherapy.

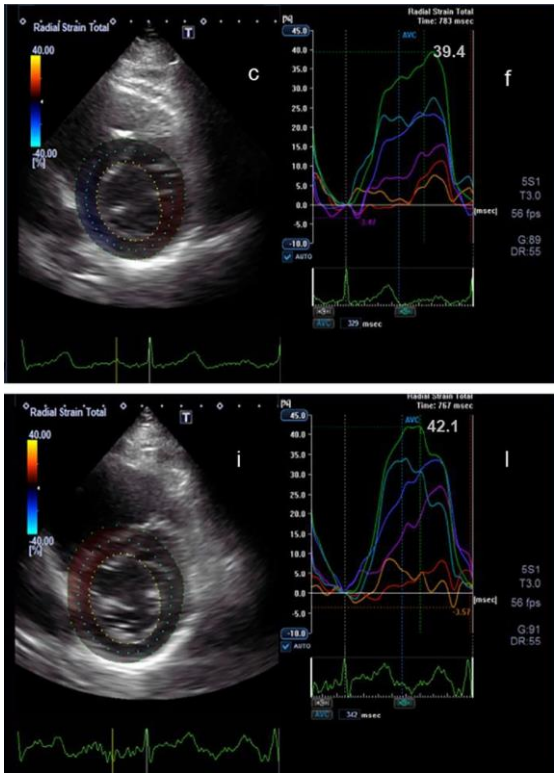

Figure 13. 2D parasternal short axis view at the level of the mitral valve (c) and the corresponding radial strain curves (f) before chemotherapy are shown. Below the corresponding view (i) and the radial strain curves (l) during chemotherapy at 3 months follow-up are presented. The peak radial strain is 39.4% and 42.1% at the beginning of chemotherapy and 3 months after, respectively.

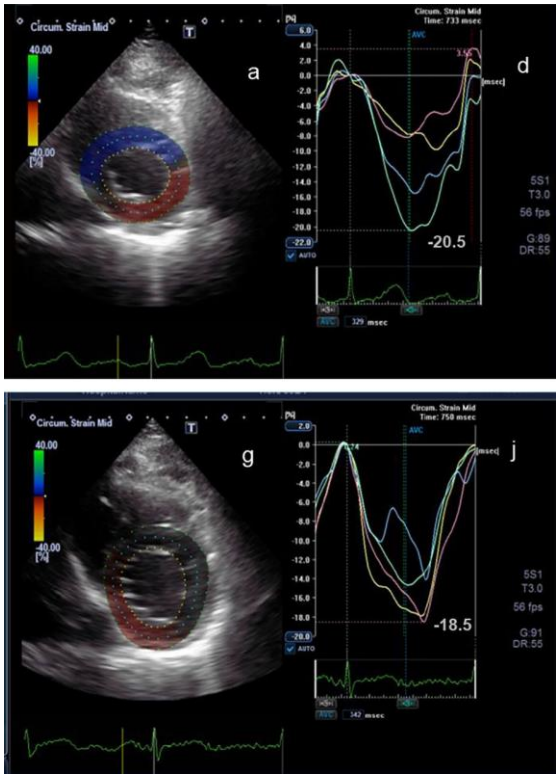

Figure 14. 2D parasternal short axis view at the level of the left ventricular apex (a) and the corresponding circumferential strain curves (d) before chemotherapy are shown. Below the corresponding view (g) and the circumferential strain curves (j) during chemotherapy at 3 months follow-up are presented. The peak circumferential strain is −20.5% and −18.5% at the beginning of chemotherapy and 3 months after, respectively.

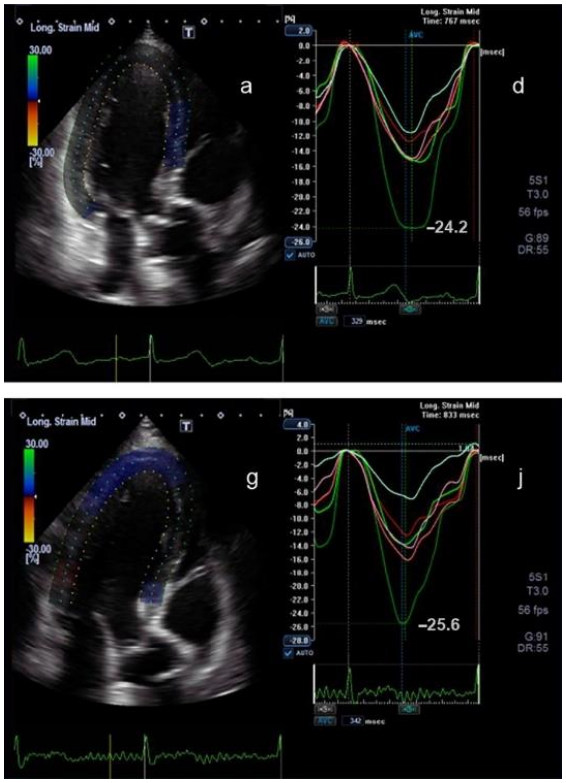

Figure 15. 2D apical long axis view (a) and the corresponding longitudinal strain curves (d) before chemotherapy are shown. Below the corresponding view (g) and the longitudinal strain curves (j) during chemotherapy at 3 months follow-up are presented. The peak longitudinal strain is −24.2% and −25.6% at the beginning of chemotherapy and 3 months after, respectively.

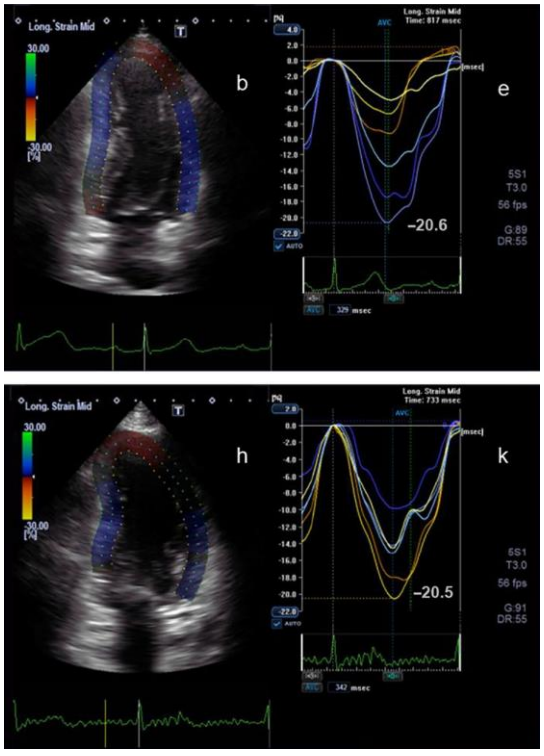

Figure 16. 2D apical two-chamber view (b) and the corresponding longitudinal strain curves (e) before chemotherapy are shown. Below the corresponding view (h) and the longitudinal strain curves (k) during chemotherapy at 3 months follow-up are presented. The peak longitudinal strain is −20.6% and −20.5% at the beginning of chemotherapy and 3 months after, respectively.

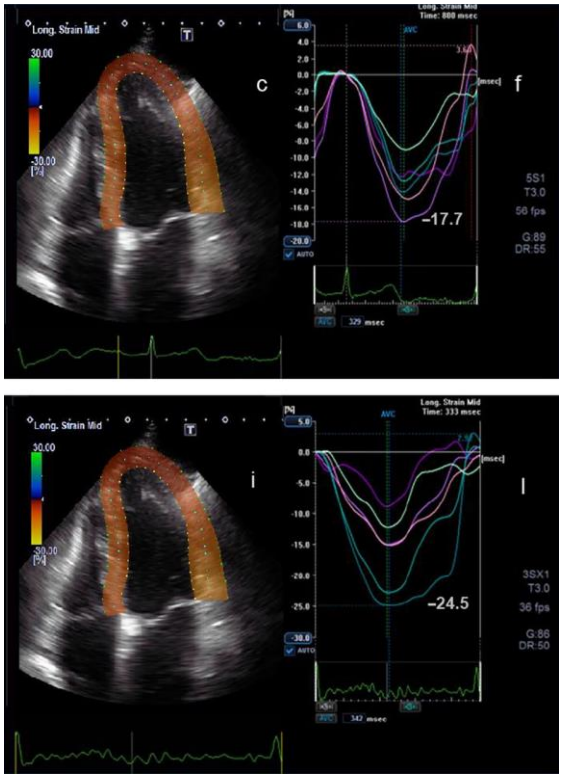

Figure 17. 2D apical four-chamber view (c) and the corresponding longitudinal strain curves (f) before chemotherapy are shown. Below the corresponding view (i) and the longitudinal strain curves (l) during chemotherapy at 3 months follow-up are presented. The peak longitudinal strain is −17.7% and −24.5% at the beginning of chemotherapy and 3 months after, respectively.

In contrast, no differences were observed in group 2 before and during chemotherapy. Three-dimensional radial, circumferential and longitudinal strain curves are shown in Figure 18.

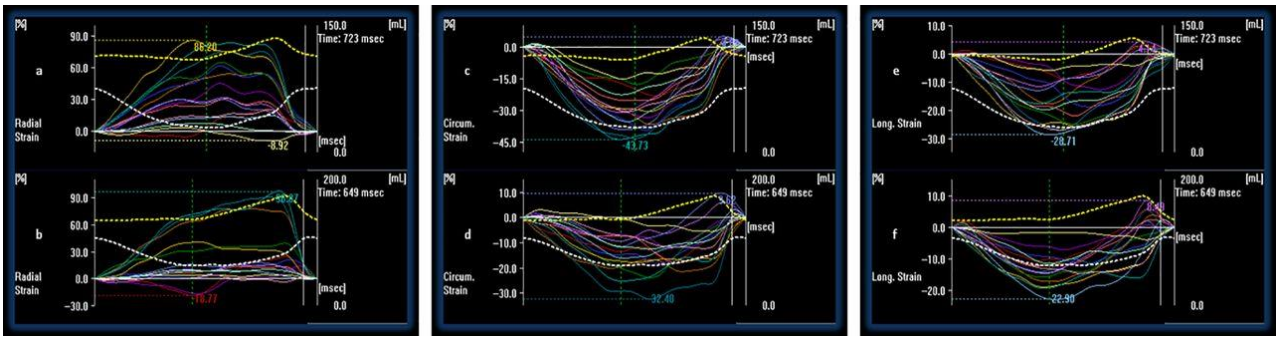

Figure 18. 3D radial strain curves of a patient before (a) and during (b) chemotherapy at 3 months follow-up are shown. 3D circumferential strain curves of a patient before (c) and during (d) chemotherapy at 3 months follow-up are presented. 3D longitudinal strain curves of a patient before (e) and during (f) chemotherapy at 3 months follow-up are demonstrated.

A subgroup analysis was additionally performed by 3D ST in patients treated with anthracycline (*n*=7). There was no difference between baseline and 3-month follow-up values (global radial strain: 31.12±9.23 vs 29.85±18.46, global circumferential strain: 23.31±4.21 vs −22.87±4.10,

global longitudinal strain: −12.56±2.45 vs −12.72±2.91). For 3D rotation, 3D twist and 3D time-to-peak intervals, no significant differences were seen (Table 6).
Intra-observer and inter-observer variabilities of strain measurements were 4.1±1.9% and 6.1±1.8%, respectively.

6 Discussion

6.1 Discussion of the study evaluating the impact of foreshortening

In recent years several recommendations for standardised conventional, and 2 and 3 dimensional speckle tracking have been published [2, 67]. It has become clear how important standardisation is for reproducibility and follow-up in healthy subjects and special patient groups, as well as in the perioperative setting [68] and emergency care [69]. The standardisation of examinations has also made it possible to establish reference values for new imaging modalities such as speckle tracking [70–73]. Exclusively, by documenting the correct geometry with standardised views is the examiner able to use the accurate mathematical models of the software for the evaluation of classical 2D parameters [74–76]. Reconstruction of non-foreshortened 2D images, acquired by 3D full volume, is possible, but does not result in significant improvement in image geometry or LV parameter assessment [77].

To this date, this is the first study to investigate the effect of foreshortening on deformation assessments. We have analysed changes in global and regional longitudinal deformation measurements due to foreshortening. In clinical practice foreshortening is often observed. In this case the apex is not directly below the transducer. In foreshortening the transducer position is frequently located too medial and/or cranial with respect to the proper apical scanning position. The out-of-plane motion during the cardiac cycle can lead to foreshortening as well [78]. The effect of foreshortening does not significantly differ in patients with normal wall motion patterns if the strain is analysed with TVI (Figure 19).

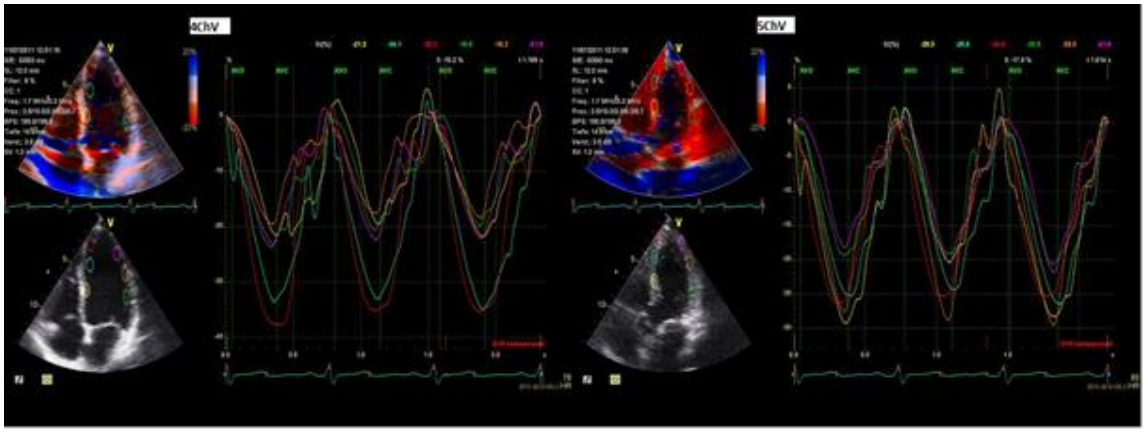

Figure 19. ***TVI based strain by 4ChV and 5ChV*** The **left panel** shows the 4ChV and the segmental longitudinal strain curves and the **right panel** illustrates the 5 ChV and the segmental longitudinal strain curves. There is no significant difference between the measurements analysed by TVI.

As TVI is angle dependent, and the fiber architecture of the basal LV regions are assumed to be similar between the inferoseptal and anteroseptal regions, the longitudinal strain seems not to be significantly influenced by a foreshortening of about 5-10 degrees. It was previously reported that the effect of angular error on strain values was very small and the largest differences were found in the apical segments [79]. Nevertheless, the effect of the alteration of the scanning plane on TVI parameters is still under discussion [80, 81].

The difference between TVI parameters (such as strain), measured in the basal septal regions by 4ChV and 5ChV, cannot be explained by the alteration of the scanning plane, but by the changes of the location of specific strains in two completely different regions (Figure 20).

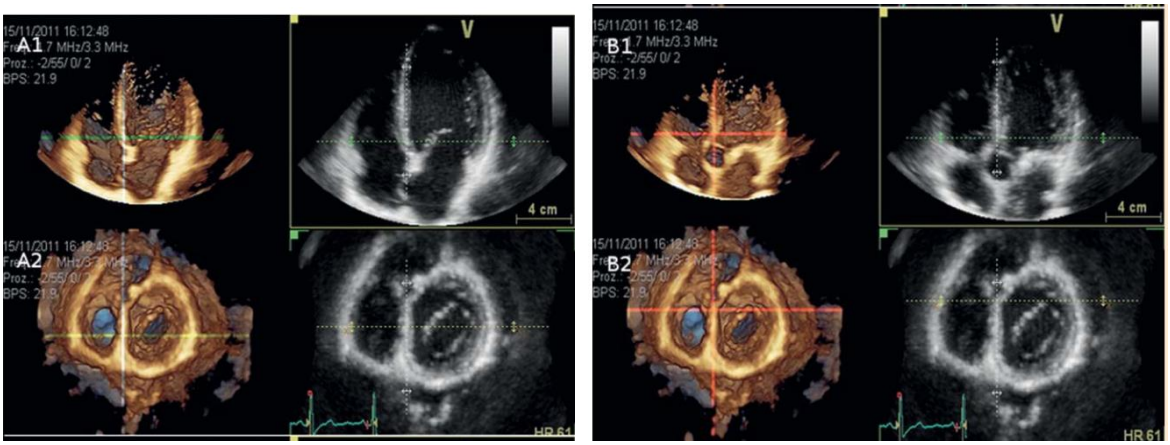

Figure 20. ***Scheme of scanning planes using the standardised 4ChV and the defined foreshortened view*** This scheme illustrates the different locations of basal strain segments, assessed by the 4ChV or the defined foreshortened view. Views A1-A2 are standardised 4ChV, while views B1-B2 are foreshortened views. Views A2 and B2 are the short axis views extending from the centre to the base of the heart. The green (on images A) and red (on images B) crosses indicate the basal septal region of the 4ChV and the defined foreshortened view, respectively.

Although we assumed that the Doppler-derived strain values of the basal regions, seen in 4ChV and 5ChV, would not differ significantly due to the similar fibre architecture, the speckle tracking-derived PSS values of the basal septal regions were still significantly lower in the standard 4ChV due to foreshortening, compared to the basal inferoseptal regions (Figure 21). This can be explained mainly by methodological issues like the signal drift in TVI or the speckle tracking quality in different basal regions.

The importance of these findings is the detection of quantitative strain differences even in a cohort of normal hearts. It can be definitely assumed that in cohorts of pathological LV contraction the differences would be more pronounced resulting in possible wrong interpretation of regional LV deformation.

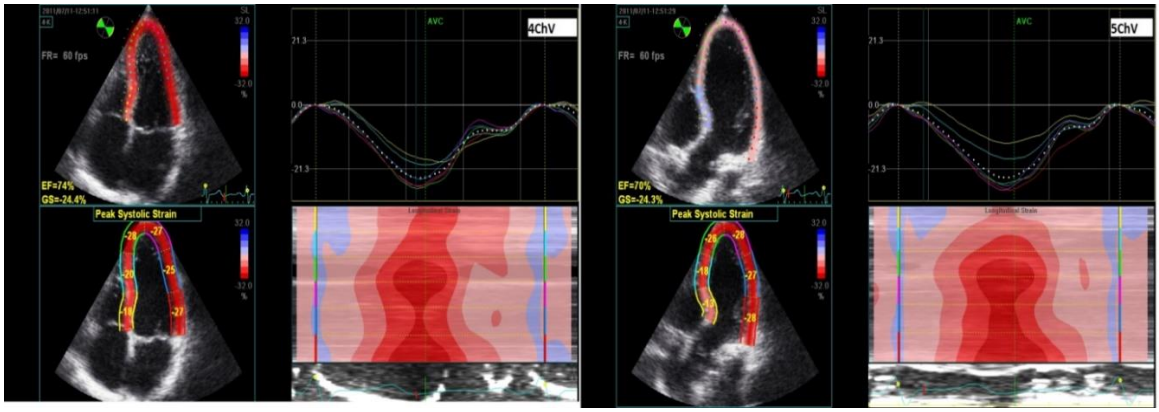

Figure 21. ***2D speckle tracking based strain*** The PSS of basal septal segment changes significantly due to foreshortening.

Tissue velocity decreases from the base to the apex because the base moves with a higher velocity, compared to the nearly stationary motion of the apex close to the transducer [82]. Strain rate and strain also show a slight gradient between basal and apical septal regions with lower values at the base [70, 83–85]. Myocardial global and segmental longitudinal PSS of normal patients was studied in the HUNT study, which found lower strain parameters in the anteroseptal than the inferoseptal region, however, these were non-significant differences [86]. Another study of a large cohort of normal probands found the same result in the septal basal region [83]. It is likely that the closeness of the basal segments to the annulus fibrosus also plays a role in this phenomenon as the strain value of fibrotic tissues is obviously lower (less negative) due to their higher rigidity. However, we explicitly emphasised when calculating the strain values in our study that the tracking area should not exceed the plane of the annulus fibrosus in the direction of the atria. The differences between the basal strain values of the inferoseptal (4ChV) and anteroseptal regions (5ChV) can be unambiguously explained by their different location. This demonstrates the importance of standardised views in speckle tracking. At the time of data acquisition, there was no valid rule for foreshortening. This was clarified later in publications [18]. Apical foreshortened images, acquired by the inappropriate positioning of the transducer, show a reduced LV length and a marked thickening of the apex with almost intact basal parts. In our present methodological scenario, the transducer was just tilted on an apical point without altering the exact location. The tilting of the transducer results in foreshortening. However, by tilting the scanning plane on the contact surface, an entirely new basal region can be viewed, and the specific region corresponds to the tilting angle.

Through our precise approach, i.e., by artificially changing the image to achieve the required foreshortened view, another region can be detected and the regional strain values also alter. Therefore, it is expected that the results of the measurement will also vary significantly. In contrast to other regions of the heart, the regional basal PSS is influenced by methodological issues, and the regional differences of PSS vary between speckle tracking and TVI as well. The basal septal strain values did not differ between the standardised and foreshortened views when strain was measured by TVI. TVI is a Doppler technique and thus angle-dependent. The minor changes of the Doppler angle can influence tissue velocity measurements resulting in variances. In addition, the signal drift in TVI can affect the strain calculation, thus strain calculated by the differences of tissue velocities, also varies pronouncedly. Due to this methodological aspect and the oblique fiber architecture of the inferoseptal and anteroseptal regions, differences of regional longitudinal strains between the two regions may not reach statistical significance despite the region of interest for basal strain measurements by TVI is definitively in two completely different basal regions. It can be declared that the physiological differences will not be detected by TVI in our analysis. Therefore, in case of a homogeneous deformation pattern, acquired by 2D speckle tracking, foreshortening results in different systolic longitudinal peak values due to the scanning of different regions of the basal septum. Two-dimensional speckle tracking is able to detect these differences between ventral and dorsal basal septal PSS values. These findings confound the evidence that the intentional alteration of the transducer position was carried out precisely. Through our intervention to achieve consistent foreshortening, we have demonstrated a methodologic effect on strain values corresponding to a change in the basal regional PSS value. The effect of 2D speckle tracking was largest near the base, which is in discordance with a study that has investigated the effect of apical foreshortening on segmental strain measurements, and has found that only the apical segments of the myocardium were affected [18]. However, in this publication the foreshortening was evoked by the inappropriate positioning of the transducer, and therefore, the alteration of the scanning region was more apically affected. In our study it is the anterior tilting of the imaging plane on a stable apical point that induces foreshortening. Both techniques can be used to create foreshortening leading to significant shortening of the left ventricular axis compared to its original size.

The 2D speckle tracking method demonstrates that the incorrect segmental planes can lead to unreliable results both in healthy cases and pathological conditions. As a result, an infarcted region may not be detected. In patients with lateral or septal regional wall motion abnormalities,

brought on by myocardial infarction (MI), the PSS values of the ischemic area were lower in the standard 4ChV than 5ChV. Thus, the infarcted region with reduced strain disappeared when the scanning plane was applied to the infarcted penumbra (Figure 22).

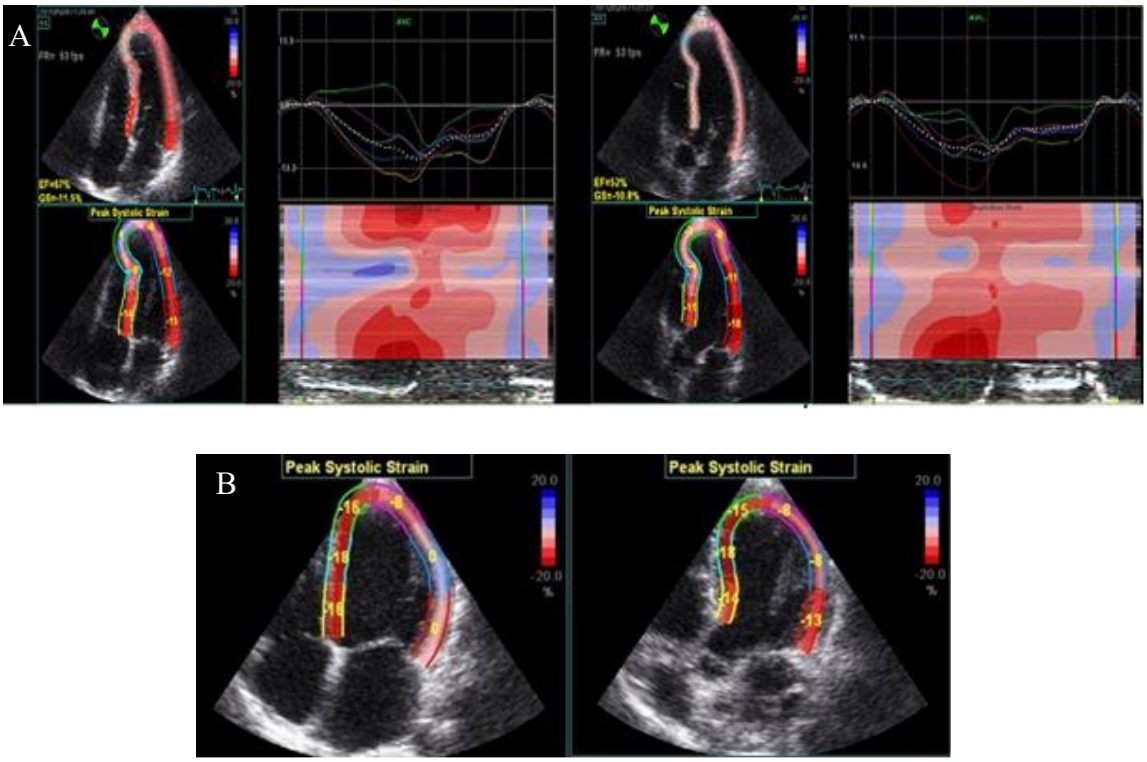

Figure 22. ***Illustration of the significant alterations of regional PSS values in septal (A) and lateral (B) myocardial infarction due to foreshortening***

In patients with normal wall motion patterns, forward bending has no effect on the global PSS, measured by either method. This case our results are in contrast with the aforementioned study. Again, this can be explained by the differences of the two techniques as the basal PSS strain values are lower than the apical ones, and foreshortening affected only the basal region in our study. Obviously, if the higher values of the apical regions change significantly, this will have a greater impact on the global strain value and thus, significant changes will be obtained.

It is essential to avoid foreshortening and to ensure standardisation, because regional PSS values differ significantly even in normal hearts. According to expert opinion, 3D echocardiography eliminates errors related to foreshortening [87]. Machine learning could play an important role in the standardisation of image capturing and image analysis in the future [88].

6.2 Discussion of the study evaluating the early detection of cardiotoxicity

In clinical practice LVEF has been the commonly used parameter to detect damages in the heart evoked by chemotherapy. As the reproducibility of LVEF estimation by 2D methods is >10%, attention is now turning to the 3D techniques and the determination of more robust global strain values [89]. Stoodley *et al.* have observed reduced global and regional longitudinal and radial strains 1 week after anthracycline treatment without detecting a change in LVEF [90]. In the present study 2D radial strain was reduced just 3 months after the beginning of chemotherapy, which suggests that 2D radial strain seems to be an early predictor of myocardial damage even in patients with already reduced LVEF. Most of the longitudinal muscle fibres are usually located in the subendomyocardial layers, especially represented by longitudinal strain. The circular muscle fibres are located in the subepimyocardial layers, mainly represented by the circular strain [63, 91, 92]. Radial strain is the result of longitudinal and circumferential fiber contraction. Methodologically however, the summation of both longitudinal and circumferential strain vectors is characterised by the so-called area strain. A higher variability in comparison to the longitudinal and circumferential strain values was observed in the radial strain measurements, which may be the consequence of the described different orientation of the myocardial fibres. However, there is no muscle fibre in the radial direction. The higher variability of radial strain, compared to longitudinal strain, may be explained by methodological issues such as spatial resolution or vendor specificity. In clinical practice the assessment of global longitudinal strain has prevailed over the years, and now global longitudinal strain assessment, measured by speckle tracking, is well established in the literature [93]. Circumferential and radial strain variations have also been reported, but more data are available for longitudinal strain, which is technically easier to measure using the apical approach.

In our study changes of global radial strain were first observed just after 3 months. This could be explained by high prerequisites on standardisation and by the inclusion of patients exclusively with excellent image quality. In other studies, myocardial deformation might have been assessed in subjects with both poor and excellent image quality.

By 2D and 3D ST analysis, remarkable differences were observed between controls (group 1) and patients (group 2). Variability was lower and reproducibility was higher regarding 3D ST because the apical sectional planes can be better standardised.

Although the longitudinal deformation, calculated from the apical views in our measurements, seems to be more similar for both techniques, there were significant differences in 2D and 3D

radial and 3D circumferential strains between controls (group 1) and patients (group 2) before chemotherapy. According to our results, circumferential strain values were lower, while radial strain values were higher by 3D ST, compared to 2D ST (Table 6). A methodological reason is presumably due to the different spatial resolution of the two methods. During the measurements of circumferential and radial strain, acquired from the parasternal view, an out-of-plane motion was generated. Due to the twisting of the cardiac motion the speckles at baseline – the R-wave of the cardiac cycle – could not be tracked over the complete cardiac cycle in contrast to 3D echocardiography [92]. As the differences between 2D and 3D speckle tracking are not homogeneous for radial strain, and the values are quite low, these observations may also be explained by methodological issues of resolution, different vendor-specific software algorithms, and smaller left ventricular cavities of the study subjects.

In the present study, the mean values of 3D radial and 3D circumferential deformation were reduced in the patient group at baseline indicating a possible impact of the tumour on the heart, and suggesting that patients with already reduced myocardial function were recruited. We found a slight, but not significant reduction in 3D global longitudinal and radial strains after 3 months of chemotherapy. Yet, due to the limited spatial and temporal resolution of 3D speckle tracking, no significant changes were detected within the first 3 months of cancer treatment. Inappropriate foreshortening views can obviously be avoided by simultaneously acquired standardised sectional planes. However, 3D ST has more artefacts and different results, compared to 2D ST, even if the same frame rates are used. For modern parameters, e.g., rotation and twist, no differences were seen. This may be explained by the fact that rotation and strain is calculated by circumferential deformation at different levels of LV short axis, which presumably can track the speckles in 2D parasternal short axis views with a similar quality than the voxels within a 3D data set. Mavinkurve-Groothuis *et al.* have observed an increase in time-to-peak interval after 3 months of anthracycline chemotherapy. In contrast to their findings, changes in 3D rotation, twist or time-to-peak interval could not be detected after 3 months in the present study [94].

In conclusion, more advanced echocardiographic techniques – in particular, the imaging of myocardial deformation by speckle-tracking strain analysis – have great potential for detecting early myocardial damage in subclinical lesions of asymptomatic oncology patients.

Limitations of early detection of cardiotoxicity:

The main limitation of the study is the small sample size and the inhomogeneity of the distribution of chemotherapeutic agents. For this reason, further subgroup analysis such as the effect of the different anti-cancer drugs on LV function, might not show relevant results. An additional limitation of our study is that controls and patients exclusively with excellent image quality were included. Thus, complete myocardial follow-up of all left ventricular segments could be achieved in these data sets. Presumably, in other studies myocardial deformation was assessed in subjects with both poor and excellent image quality.

7 New observations

Compared to TVI, it may be easier to detect differences between regional LV deformations by 2D speckle tracking, however, the prerequisite is an adequate image quality. In contrast, TVI can be rated as a more robust technique in patients with inadequate acoustic windows. It is essential to avoid foreshortening and to ensure standardisation. If these prerequisites are not fulfilled, even normal regional PSS values differ significantly.

Preclinical myocardial dysfunction, induced by cardiotoxic chemotherapy, can be detected by the deformation parameters of ST.

We suggest that 2D global radial strain is also helpful as potential parameter to detect early myocardial damage during chemotherapy already after 3 months.

8 Summary

A high methodological precision to ensure standardisation is required for adequate image acquisition in advanced echocardiography with the application of modern post-processing tools like 2D- and 3D ST in clinical routine. Further advances in technology - especially 3D echocardiography with improved spatial resolution - will allow the production of standardised sectional planes in post-processing, which could be a useful adjunct to routine examinations in the future. Deformation imaging is already a perfect complement to conventional LV-EF evaluations and together with speckle tracking, they definitively have replaced conventional LV-EF evaluations for the detection of subclinical lesions.

9 References

1. Hagendorff A. Transthoracic echocardiography in adult patients--a proposal for documenting a standardized investigation. Ultraschall Med. 2008;29:344-65.
2. Galderisi M, Cosyns B, Edvardsen T, Cardim N, Delgado V, Di Salvo G, et al. Standardization of adult transthoracic echocardiography reporting in agreement with recent chamber quantification, diastolic function, and heart valve disease recommendations: an expert consensus document of the European Association of Cardiovascular Imaging. Eur Heart J Cardiovasc Imaging. 2017;18:1301–10.
3. Badano LP, Kolias TJ, Muraru D, Abraham TP, Aurigemma G, Edvardsen T, et al. Standardization of left atrial, right ventricular, and right atrial deformation imaging using two-dimensional speckle tracking echocardiography: a consensus document of the EACVI/ASE/Industry Task Force to standardize deformation imaging. Eur Heart J Cardiovasc Imaging. 2018;19:591–600.
4. Kou S, Caballero L, Dulgheru R, Voilliot D, Sousa C de, Kacharava G, et al. Echocardiographic reference ranges for normal cardiac chamber size: results from the NORRE study. Eur Heart J Cardiovasc Imaging. 2014;15:680–90.
5. Shiino K, Yamada A, Ischenko M, Khandheria BK, Hudaverdi M, Speranza V, et al. Intervendor consistency and reproducibility of left ventricular 2D global and regional strain with two different high-end ultrasound systems. Eur Heart J Cardiovasc Imaging. 2017;18:707–16.
6. Sengupta PP, Korinek J, Belohlavek M, Narula J, Vannan MA, Jahangir A, Khandheria BK. Left ventricular structure and function: basic science for cardiac imaging. J Am Coll Cardiol. 2006;48:1988–2001.
7. Nakatani S. Left ventricular rotation and twist: why should we learn? J Cardiovasc Ultrasound. 2011;19:1–6.
8. Marwick TH, Yu C-M, Sun J. Myocardial imaging: Tissue doppler and speckle tracking. Malden, Mass.: Blackwell Pub; 2007.
9. Bijnens B, Cikes M, Butakoff C, Sitges M, Crispi F. Myocardial motion and deformation: What does it tell us and how does it relate to function? Fetal Diagn Ther. 2012;32:5–16.
10. Lengyel M, Asbóth R. Echocardiographia. Budapest: Medicina; 2012.
11. Opdahl A, Helle-Valle T, Skulstad H, Smiseth OA. Strain, strain rate, torsion, and twist: echocardiographic evaluation. Curr Cardiol Rep. 2015;17:568.

12. Stoebe S, Tarr A, Pfeiffer D, Hagendorff A. The impact of the width of the tracking area on speckle tracking parameters-methodological aspects of deformation imaging. Echocardiography. 2014;31:586–96.
13. Blessberger H, Binder T. NON-invasive imaging: Two dimensional speckle tracking echocardiography: basic principles. Heart. 2010;96:716–22.
14. Muraru D, Niero A, Rodriguez-Zanella H, Cherata D, Badano L. Three-dimensional speckle-tracking echocardiography: benefits and limitations of integrating myocardial mechanics with three-dimensional imaging. Cardiovasc Diagn Ther. 2018;8:101–17.
15. Thomas JD, Badano LP. EACVI-ASE-industry initiative to standardize deformation imaging: a brief update from the co-chairs. Eur Heart J Cardiovasc Imaging. 2013;14:1039–40.
16. Farsalinos KE, Daraban AM, Ünlü S, Thomas JD, Badano LP, Voigt J-U. Head-to-Head Comparison of Global Longitudinal Strain Measurements among Nine Different Vendors: The EACVI/ASE Inter-Vendor Comparison Study. J Am Soc Echocardiogr. 2015;28:1171-1181, e2.
17. Voigt J-U, Pedrizzetti G, Lysyansky P, Marwick TH, Houle H, Baumann R, et al. Definitions for a common standard for 2D speckle tracking echocardiography: consensus document of the EACVI/ASE/Industry Task Force to standardize deformation imaging. European Heart Journal - Cardiovascular Imaging. 2015;16:1–11.
18. Ünlü S, Duchenne J, Mirea O, Pagourelias ED, Bézy S, Cvijic M, et al. Impact of apical foreshortening on deformation measurements: a report from the EACVI-ASE Strain Standardization Task Force. European Heart Journal - Cardiovascular Imaging. 2020;21:337–43.
19. Smistad E, Ostvik A, Salte IM, Melichova D, Nguyen TM, Haugaa K, et al. Real-Time Automatic Ejection Fraction and Foreshortening Detection Using Deep Learning. IEEE Trans Ultrason Ferroelectr Freq Control. 2020;67:2595–604.
20. Siegel RL, Miller KD, Jemal A. Cancer statistics, 2019. CA Cancer J Clin. 2019;69:7–34.
21. Cramer L, Hildebrandt B, Kung T, Wichmann K, Springer J, Doehner W, et al. Cardiovascular function and predictors of exercise capacity in patients with colorectal cancer. J Am Coll Cardiol. 2014;64:1310–9.
22. Anker MS, Ebner N, Hildebrandt B, Springer J, Sinn M, Riess H, et al. Resting heart rate is an independent predictor of death in patients with colorectal, pancreatic, and non-small

cell lung cancer: results of a prospective cardiovascular long-term study. European journal of heart failure. 2016;18:1524–34.

23. Hu S, Lou J, Zhang Y, Chen P. Low heart rate variability relates to the progression of gastric cancer. World J Surg Oncol. 2018;16:49.
24. Guo Y, Koshy S, Hui D, Palmer JL, Shin K, Bozkurt M, Yusuf SW. Prognostic Value of Heart Rate Variability in Patients With Cancer. J Clin Neurophysiol. 2015;32:516–20.
25. Belloum Y, Rannou-Bekono F, Favier FB. Cancer-induced cardiac cachexia: Pathogenesis and impact of physical activity (Review). Oncol Rep. 2017;37:2543–52.
26. Kanda T, Takahashi T. Interleukin-6 and cardiovascular diseases. Jpn Heart J. 2004;45:183–93.
27. Razeghi P, Young ME, Alcorn JL, Moravec CS, Frazier OH, Taegtmeyer H. Metabolic gene expression in fetal and failing human heart. Circulation. 2001;104:2923–31.
28. Willis MS, Schisler JC, Li L, Rodríguez JE, Hilliard EG, Charles PC, Patterson C. Cardiac muscle ring finger-1 increases susceptibility to heart failure in vivo. Circ Res. 2009;105:80–8.
29. Willis MS, Rojas M, Li L, Selzman CH, Tang R-H, Stansfield WE, et al. Muscle ring finger 1 mediates cardiac atrophy in vivo. Am J Physiol Heart Circ Physiol. 2009;296:H997-H1006.
30. Schäfer M, Oeing CU, Rohm M, Baysal-Temel E, Lehmann LH, Bauer R, et al. Ataxin-10 is part of a cachexokine cocktail triggering cardiac metabolic dysfunction in cancer cachexia. Molecular Metabolism. 2016;5:67–78.
31. Kerkhofs M, Bittremieux M, Morciano G, Giorgi C, Pinton P, Parys JB, Bultynck G. Emerging molecular mechanisms in chemotherapy: Ca2+ signaling at the mitochondria-associated endoplasmic reticulum membranes. Cell Death Dis. 2018;9:334.
32. Han X, Zhou Y, Liu W. Precision cardio-oncology: understanding the cardiotoxicity of cancer therapy. NPJ Precis Oncol. 2017;1:31.
33. Tacar O, Sriamornsak P, Dass CR. Doxorubicin: an update on anticancer molecular action, toxicity and novel drug delivery systems. J Pharm Pharmacol. 2013;65:157–70.
34. Lehmann LH, Fröhling S. Mechanismen der Kardiotoxizität onkologischer Therapien. [Mechanisms of cardiotoxicity of oncological therapies]. Internist (Berl). 2020;61:1132–9.

35. Felker GM, Thompson RE, Hare JM, Hruban RH, Clemetson DE, Howard DL, et al. Underlying causes and long-term survival in patients with initially unexplained cardiomyopathy. N Engl J Med. 2000;342:1077–84.
36. Cardinale D, Colombo A, Bacchiani G, Tedeschi I, Meroni CA, Veglia F, et al. Early detection of anthracycline cardiotoxicity and improvement with heart failure therapy. Circulation. 2015;131:1981–8.
37. Zamorano JL, Lancellotti P, Rodriguez Muñoz D, Aboyans V, Asteggiano R, Galderisi M, et al. 2016 ESC Position Paper on cancer treatments and cardiovascular toxicity developed under the auspices of the ESC Committee for Practice Guidelines: The Task Force for cancer treatments and cardiovascular toxicity of the European Society of Cardiology (ESC). Eur Heart J. 2016;37:2768–801.
38. Nemeth BT, Varga ZV, Wu WJ, Pacher P. Trastuzumab cardiotoxicity: from clinical trials to experimental studies. Br J Pharmacol. 2017;174:3727–48.
39. Ozcelik C, Erdmann B, Pilz B, Wettschureck N, Britsch S, Hübner N, et al. Conditional mutation of the ErbB2 (HER2) receptor in cardiomyocytes leads to dilated cardiomyopathy. Proc Natl Acad Sci U S A. 2002;99:8880–5.
40. Gottdiener JS. Cardiotoxicity Associated With High-Dose Cyclophosphamide Therapy. Arch Intern Med. 1981;141:758.
41. Madeddu C, Deidda M, Piras A, Cadeddu C, Demurtas L, Puzzoni M, et al. Pathophysiology of cardiotoxicity induced by nonanthracycline chemotherapy. Journal of Cardiovascular Medicine. 2016;17:e12-e18.
42. Chowdhury S, Sinha K, Banerjee S, Sil PC. Taurine protects cisplatin induced cardiotoxicity by modulating inflammatory and endoplasmic reticulum stress responses. Biofactors. 2016;42:647–64.
43. El-Awady E-SE, Moustafa YM, Abo-Elmatty DM, Radwan A. Cisplatin-induced cardiotoxicity: Mechanisms and cardioprotective strategies. Eur J Pharmacol. 2011;650:335–41.
44. Wu P, Oren O, Gertz MA, Yang EH. Proteasome Inhibitor-Related Cardiotoxicity: Mechanisms, Diagnosis, and Management. Curr Oncol Rep. 2020;22:66.
45. Force T, Krause DS, van Etten RA. Molecular mechanisms of cardiotoxicity of tyrosine kinase inhibition. Nat Rev Cancer. 2007;7:332–44.

46. Giudice V, Vecchione C, Selleri C. Cardiotoxicity of Novel Targeted Hematological Therapies. Life (Basel) 2020.
47. Ganatra S, Sharma A, Shah S, Chaudhry GM, Martin DT, Neilan TG, et al. Ibrutinib-Associated Atrial Fibrillation. JACC Clin Electrophysiol. 2018;4:1491–500.
48. Wang Y. Mitogen-activated protein kinases in heart development and diseases. Circulation. 2007;116:1413–23.
49. Thyss A, Gaspard MH, Marsault R, Milano G, Frelin C, Schneider M. Very high endothelin plasma levels in patients with 5-FU cardiotoxicity. Ann Oncol. 1992;3:88.
50. Tsibiribi P, Bui-Xuan C, Bui-Xuan B, Lombard-Bohas C, Duperret S, Belkhiria M, et al. Cardiac lesions induced by 5-fluorouracil in the rabbit. Hum Exp Toxicol. 2006;25:305–9.
51. Saif MW, Shah MM, Shah AR. Fluoropyrimidine-associated cardiotoxicity: revisited. Expert Opin Drug Saf. 2009;8:191–202.
52. Michel L, Totzeck M, Lehmann L, Finke D. Zunehmende Relevanz von Immuncheckpoint-Inhibitoren und deren Bedeutung für das kardiovaskuläre System. [Emerging role of immune checkpoint inhibitors and their relevance for the cardiovascular system]. Herz. 2020;45:645–51.
53. Moslehi JJ, Salem J-E, Sosman JA, Lebrun-Vignes B, Johnson DB. Increased reporting of fatal immune checkpoint inhibitor-associated myocarditis. The Lancet. 2018;391:933.
54. López-Sendón J, Álvarez-Ortega C, Zamora Auñon P, Buño Soto A, Lyon AR, Farmakis D, et al. Classification, prevalence, and outcomes of anticancer therapy-induced cardiotoxicity: the CARDIOTOX registry. Eur Heart J. 2020;41:1720–9.
55. Appell PG, Rüssel J, Bethge S, Schlitt A. Kardiotoxizität onkologischer Therapien (1): Myokardiale Dysfunktion und Herzinsuffizienz. Deutsches Aerzteblatt Online 2018.
56. Gaggin HK, Januzzi JL. The past, the present, and the future of natriuretic peptides in the diagnosis of heart failure. European Heart Journal Supplements. 2018;20:G11-G20.
57. Michel L, Rassaf T, Totzeck M. Biomarkers for the detection of apparent and subclinical cancer therapy-related cardiotoxicity. J Thorac Dis. 2018;10:S4282-S4295.
58. Hammarsten O, Mair J, Möckel M, Lindahl B, Jaffe AS. Possible mechanisms behind cardiac troponin elevations. Biomarkers. 2018;23:725–34.
59. Michel L, Mincu RI, Mahabadi AA, Settelmeier S, Al-Rashid F, Rassaf T, Totzeck M. Troponins and brain natriuretic peptides for the prediction of cardiotoxicity in cancer patients: a meta-analysis. European journal of heart failure. 2020;22:350–61.

60. Pudil R, Mueller C, Čelutkienė J, Henriksen PA, Lenihan D, Dent S, et al. Role of serum biomarkers in cancer patients receiving cardiotoxic cancer therapies: a position statement from the Cardio-Oncology Study Group of the Heart Failure Association and the Cardio-Oncology Council of the European Society of Cardiology. European journal of heart failure. 2020;22:1966–83.
61. Hoffmann R, Altiok E, Friedman Z, Becker M, Frick M. Myocardial deformation imaging by two-dimensional speckle-tracking echocardiography in comparison to late gadolinium enhancement cardiac magnetic resonance for analysis of myocardial fibrosis in severe aortic stenosis. The American journal of cardiology. 2014;114:1083–8.
62. Thavendiranathan P, Negishi T, Somerset E, Negishi K, Penicka M, Lemieux J, et al. Strain-Guided Management of Potentially Cardiotoxic Cancer Therapy. J Am Coll Cardiol. 2021;77:392–401.
63. Evangelista A, Flachskampf F, Lancellotti P, Badano L, Aguilar R, Monaghan M, et al. European Association of Echocardiography recommendations for standardization of performance, digital storage and reporting of echocardiographic studies. Eur J Echocardiogr. 2008;9:438–48.
64. Douglas PS, Khandheria B, Stainback RF, Weissman NJ, Brindis RG, Patel MR, et al. ACCF/ASE/ACEP/ASNC/SCAI/SCCT/SCMR 2007 appropriateness criteria for transthoracic and transesophageal echocardiography: a report of the American College of Cardiology Foundation Quality Strategic Directions Committee Appropriateness Criteria Working Group, American Society of Echocardiography, American College of Emergency Physicians, American Society of Nuclear Cardiology, Society for Cardiovascular Angiography and Interventions, Society of Cardiovascular Computed Tomography, and the Society for Cardiovascular Magnetic Resonance. Endorsed by the American College of Chest Physicians and the Society of Critical Care Medicine. J Am Soc Echocardiogr. 2007;20:787–805.
65. Rahmouni HW, Ky B, Plappert T, Duffy K, Wiegers SE, Ferrari VA, et al. Clinical utility of automated assessment of left ventricular ejection fraction using artificial intelligence-assisted border detection. American Heart Journal. 2008;155:562–70.
66. Mor-Avi V, Lang RM, Badano LP, Belohlavek M, Cardim NM, Derumeaux G, et al. Current and evolving echocardiographic techniques for the quantitative evaluation of cardiac mechanics: ASE/EAE consensus statement on methodology and indications

endorsed by the Japanese Society of Echocardiography. J Am Soc Echocardiogr. 2011;24:277–313.

67. Douglas PS, Carabello BA, Lang RM, Lopez L, Pellikka PA, Picard MH, et al. 2019 ACC/AHA/ASE Key Data Elements and Definitions for Transthoracic Echocardiography: A Report of the American College of Cardiology/American Heart Association Task Force on Clinical Data Standards (Writing Committee to Develop Clinical Data Standards for Transthoracic Echocardiography) and the American Society of Echocardiography. J Am Soc Echocardiogr. 2019;32:1161–248.
68. Mackensen GB, Nicoara A. Improving the Quality and Reporting of Perioperative Echocardiography. J Am Soc Echocardiogr. 2018;31:A22-A23.
69. Michels G, Busch H-J. Standardisierte fokussierte Echokardiografie in der Akutmedizin. [Standardized focused echocardiography in acute medicine]. Dtsch Med Wochenschr. 2019;144:288.
70. Levy PT, Machefsky A, Sanchez AA, Patel MD, Rogal S, Fowler S, et al. Reference Ranges of Left Ventricular Strain Measures by Two-Dimensional Speckle-Tracking Echocardiography in Children: A Systematic Review and Meta-Analysis. J Am Soc Echocardiogr. 2016;29:209-225.e6.
71. Sugimoto T, Dulgheru R, Bernard A, Ilardi F, Contu L, Addetia K, et al. Echocardiographic reference ranges for normal left ventricular 2D strain: results from the EACVI NORRE study. European Heart Journal - Cardiovascular Imaging. 2017;18:833–40.
72. Tsugu T, Postolache A, Dulgheru R, Sugimoto T, Tridetti J, Nguyen Trung M-L, et al. Echocardiographic reference ranges for normal left ventricular layer-specific strain: results from the EACVI NORRE study. European Heart Journal - Cardiovascular Imaging. 2020;21:896–905.
73. Nemes A, Kormányos Á, Kalapos A, Domsik P, Gyenes N, Ambrus N, Lengyel C. Normal reference values of left ventricular strain parameters in healthy adults: Real-life experience from the single-center three-dimensional speckle-tracking echocardiographic MAGYAR-Healthy Study. J Clin Ultrasound. 2021;49:368–77.
74. Wyatt HL, Heng MK, Meerbaum S, Hestenes JD, Cobo JM, Davidson RM, Corday E. Cross-sectional echocardiography. I. Analysis of mathematic models for quantifying mass of the left ventricle in dogs. Circulation. 1979;60:1104–13.

75. Wyatt HL, Heng MK, Meerbaum S, Gueret P, Hestenes J, Dula E, Corday E. Cross-sectional echocardiography. II. Analysis of mathematic models for quantifying volume of the formalin-fixed left ventricle. Circulation. 1980;61:1119–25.
76. Wyatt HL, Meerbaum S, Heng MK, Gueret P, Corday E. Cross-sectional echocardiography III. Analysis of mathematic models for quantifying volume of symmetric and asymmetric left ventricles. American Heart Journal. 1980;100:821–8.
77. Amzulescu MS, Slavich M, Florian A, Goetschalckx K, Voigt J-U. Does two-dimensional image reconstruction from three-dimensional full volume echocardiography improve the assessment of left ventricular morphology and function? Echocardiography. 2013;30:55–63.
78. Nesser H-J, Mor-Avi V, Gorissen W, Weinert L, Steringer-Mascherbauer R, Niel J, et al. Quantification of left ventricular volumes using three-dimensional echocardiographic speckle tracking: comparison with MRI. Eur Heart J. 2009;30:1565–73.
79. Storaa C, Aberg P, Lind B, Brodin L-A. Effect of angular error on tissue Doppler velocities and strain. Echocardiography. 2003;20:581–7.
80. Cho G-Y, Chan J, Leano R, Strudwick M, Marwick TH. Comparison of two-dimensional speckle and tissue velocity based strain and validation with harmonic phase magnetic resonance imaging. The American journal of cardiology. 2006;97:1661–6.
81. D'hooge J, Heimdal A, Jamal F, Kukulski T, Bijnens B, Rademakers F, et al. Regional strain and strain rate measurements by cardiac ultrasound: principles, implementation and limitations. Eur J Echocardiogr. 2000;1:154–70.
82. Leitman M, Lysyansky P, Sidenko S, Shir V, Peleg E, Binenbaum M, et al. Two-dimensional strain-a novel software for real-time quantitative echocardiographic assessment of myocardial function. J Am Soc Echocardiogr. 2004;17:1021–9.
83. Voigt JU, Arnold MF, Karlsson M, Hübbert L, Kukulski T, Hatle L, Sutherland GR. Assessment of regional longitudinal myocardial strain rate derived from doppler myocardial imaging indexes in normal and infarcted myocardium. J Am Soc Echocardiogr. 2000;13:588–98.
84. Reckefuss N, Butz T, Horstkotte D, Faber L. Evaluation of longitudinal and radial left ventricular function by two-dimensional speckle-tracking echocardiography in a large cohort of normal probands. Int J Cardiovasc Imaging. 2011;27:515–26.

85. Fine NM, Shah AA, Han I-Y, Yu Y, Hsiao J-F, Koshino Y, et al. Left and right ventricular strain and strain rate measurement in normal adults using velocity vector imaging: an assessment of reference values and intersystem agreement. Int J Cardiovasc Imaging. 2013;29:571–80.
86. Dalen H, Thorstensen A, Aase SA, Ingul CB, Torp H, Vatten LJ, Stoylen A. Segmental and global longitudinal strain and strain rate based on echocardiography of 1266 healthy individuals: the HUNT study in Norway. Eur J Echocardiogr. 2010;11:176–83.
87. Guta AC, Badano LP, Ochoa-Jimenez RC, Genovese D, Previtero M, Civera S, et al. Three-dimensional echocardiography to assess left ventricular geometry and function. Expert Rev Cardiovasc Ther. 2019;17:801–15.
88. Narang A, Mor-Avi V, Prado A, Volpato V, Prater D, Tamborini G, et al. Machine learning based automated dynamic quantification of left heart chamber volumes. European Heart Journal - Cardiovascular Imaging. 2019;20:541–9.
89. Thavendiranathan P, Grant AD, Negishi T, Plana JC, Popović ZB, Marwick TH. Reproducibility of echocardiographic techniques for sequential assessment of left ventricular ejection fraction and volumes: application to patients undergoing cancer chemotherapy. J Am Coll Cardiol. 2013;61:77–84.
90. Stoodley PW, Richards DAB, Hui R, Boyd A, Harnett PR, Meikle SR, et al. Two-dimensional myocardial strain imaging detects changes in left ventricular systolic function immediately after anthracycline chemotherapy. Eur J Echocardiogr. 2011;12:945–52.
91. Ho SY. Anatomy and myoarchitecture of the left ventricular wall in normal and in disease. Eur J Echocardiogr. 2009;10:iii3-7.
92. Mor-Avi V, Lang RM, Badano LP, Belohlavek M, Cardim NM, Derumeaux G, et al. Current and evolving echocardiographic techniques for the quantitative evaluation of cardiac mechanics: ASE/EAE consensus statement on methodology and indications endorsed by the Japanese Society of Echocardiography. Eur J Echocardiogr. 2011;12:167–205.
93. Thavendiranathan P, Poulin F, Lim K-D, Plana JC, Woo A, Marwick TH. Use of myocardial strain imaging by echocardiography for the early detection of cardiotoxicity in patients during and after cancer chemotherapy: a systematic review. J Am Coll Cardiol. 2014;63:2751–68.

94. Mavinkurve-Groothuis AMC, Marcus KA, Pourier M, Loonen J, Feuth T, Hoogerbrugge PM, et al. Myocardial 2D strain echocardiography and cardiac biomarkers in children during and shortly after anthracycline therapy for acute lymphoblastic leukaemia (ALL): a prospective study. European Heart Journal - Cardiovascular Imaging. 2013;14:562–9.

10 Acknowledgements

I would like to thank my thesis supervisor, Professor Albert Varga for his help in developing my scientific connections, for his faith in me, encouragement and advice during my time as a PhD student.

I express my sincere gratitude to Professor Andreas Hagendorff, my thesis supervisor in Leipzig, who supported me with patience and knowledge throughout my thesis preparation and my life in Leipzig.

I would specially thank to my colleagues and friends for their support, allowed me to complete this thesis.

I would like to dedicate this thesis to my family, my lovely husband Jan and my sweet daughter Anna, and to my parents for their understanding and love.